DOE/ER/03077-244

Courant Mathematics and
Computing Laboratory

U.S. Department of Energy

Stability of Two Dimensional Immiscible Flow to Viscous Fingering

Michael J. King, W. B. Lindquist,
and L. Reyna

NYU DOE/ER 03077-244 c.2
King, Michael J
Stability of two
dimensional immiscible

Research and Development Report

Supported by the Applied Mathematical Sciences
subprogram of the Office of Energy Research,
U.S. Dept. of Energy under Contract DE-AC02-76ER03077

Mathematics and Computers

March 1985

NEW YORK UNIVERSITY

DOE/ER/03077-244

Courant Mathematics and
Computing Laboratory

U. S. Department of Energy

Stability of Two Dimensional Immiscible Flow to Viscous Fingering

Michael J. King, W. B. Lindquist, and L. Reyna

Research and Development Report

Supported by the Applied Mathematical Sciences subprogram of the Office of Energy Research, U. S. Department of Energy under Contract DE-AC02-76ER03077

Mathematics and Computers

March 1985

New York University

UNCLASSIFIED

DOE/ER/03077-244
UC-32
Mathematics and Computers

Courant Mathematics and Computing Laboratory

New York University

Stability of Two Dimensional Immiscible Flow to Viscous Fingering

Michael J. King, W. B. Lindquist, and L. Reyna

March 1985

Supported by the Applied Mathematical Sciences subprogram of the Office of Energy Research, U. S. Department of Energy under Contract No. DE-AC02-76ER03077

UNCLASSIFIED

Table of Contents

		Page
	Abstract	1
1.	Introduction	2
2.	The Displacement Process	4
3.	The Numerical Approximation	5
4.	Analysis of Case Studies	7
	4.1 Homogenous Rock Studies	10
	4.1.1 Stability Dependence on Mobility Ratio	10
	4.1.2 Stability Dependence on Initial Finger Size	11
	4.1.3 Stability Dependence on Capillary Pressure	12
	4.1.4 Comparison with No Capillarity	12
	4.2 Studies in Heterogeneous Rock	12
5.	Conclusions	14
	Nomenclature	15
	References	16
	Figure Captions	18
	Figures	20

DISCLAIMER

This report was prepared as an account of work sponsored by an agency of the United States Government. Neither the United States Government nor any agency thereof, nor any of their employees, makes any warranty, express or implied, or assumes any legal liability or responsibility for the accuracy, completeness, or usefulness of any information, apparatus, product, or process disclosed, or represents that its use would not infringe privately owned rights. Reference herein to any specific commercial product, process, or service by trade name, trademark, manufacturer, or otherwise, does not necessarily constitute or imply its endorsement, recommendation, or favoring by the United States Government or any agency thereof. The views and opinions of authors expressed herein do not necessarily state or reflect those of the United States Government or any agency thereof.

Printed in U.S.A.

Available from

National Technical Information Service
U.S. Department of Commerce
5285 Port Royal Road
Springfield, VA 22161

Stability of Two Dimensional Immiscible Flow to Viscous Fingering

Michael J. King

Reservoir Engineering Research
Sohio Petroleum Company
Cleveland, Ohio 44128

W. B. Lindquist [1]

Courant Institute of Mathematical Sciences
New York University
New York, N.Y. 10012

L. Reyna [2]

Aerodynamisches Institut der RWTH
Weillnerstrasse zw. 5-7
5100 Aachen, West Germany

ABSTRACT

The stability of incompressible, gravity free, immiscible two phase flow to viscous fingering is studied numerically. In contrast to numerical studies in the literature, but in good qualitative agreement with laboratory studies, we find a large parameter regime for which the displacement is strongly unstable. The parameter space examined includes mobility ratio, capillary pressure strength, size of perturbation, and heterogeneity of the medium.

1. Supported by the Applied Mathematical Sciences subprogram of the Office of Energy Research, U. S. Dept. of Energy, Contract DE-AC02-76ERO3077.
2. Supported in part by the National Science Foundation, Contract MCS - 8201599.

1. Introduction

Two phase miscible and immiscible displacement processes occur in reservoir operations and in laboratory core floods. The stability of miscible and immiscible flood has been studied by phenomenological models,[1,2,3,4] numerical simulators,[5,6] and by linearized stability analyses.[1,7,8,9] In general, phenomenological models assume simplified flow descriptions so that other effects may be studied in more detail. Numerical simulation is often used but usually at a cost of large numerical diffusion effects. Linearized stability analyses provide information on the inception of instability for small perturbations but give no information on the effects of perturbation size or the eventual form of fingered profiles.

The purpose of this study is to perform a fundamental examination of the stability of immiscible flood. The usual relative permeability and capillary pressure functions are used to describe the local flow; no effective (average) "shape factors"[2,3] are assumed. Care is taken to ensure that the physical effects (capillarity, heterogeneity) dominate the numerical dispersion present in the calculation.

The instability of immiscible flow is studied instead of miscible flow for two reasons. First, it is more difficult to model numerically than miscible flood; the Buckley-Leverett mixing zone leads to enhanced stability compared to the corresponding miscible flood. Second, in addition to viscous and dispersive forces, miscible flood behavior is further complicated by the phase behavior of components, non-trivial chemical interactions between components and rock, and even regions of immiscible flow ($C0_2$ flood). In immiscible processes, the instability is dominated by flow physics (interplay of viscous and capillary effects); in many instances the effects of chemistry are of secondary importance. Therefore, the model (1) is expected to describe a realistic flood without extensive simplification of the process.

Laboratory studies of flow through core samples exhibit a variety of fingering phenomena.[1,9] Linearized analyses of two phase, incompressible, immiscible flow[6,8] reveal regimes of definite instability for the growth of viscous fingers. Published numerical studies[6] in the non linear range show little evidence of instability for even moderately strong adverse mobility ratios. *The results of our study show that understanding of the interplay of length scales present in the numerical study is essential for a correct numerical calculation of the*

stability of viscous fingering.

The problem can be characterized in terms of four dimensionless length scales:

1) $R_{cap} = L_{cap} / L$ characteristic of the capillary strength.

2) $R_{het} = L_{het} / L$ characteristic of either the heterogeneity in the medium (or characteristic of the length scale of perturbation(s) inserted in the initial data if the medium is homogeneous).

3) $R_g = L_g / L = \max(\Delta x, \Delta y) / L$ where Δx and Δy are the mesh spacings (assumed regular) of the grid.

4) $R_{dlsp} = L_{dlsp} / L$ characteristic of a minimum 'fiducial wavelength' for the numerical scheme due to inaccuracies arising from truncation error of the finite difference scheme employed.

In the above L is a reference length scale which we shall assume to be $L = \min(L_x, L_y)$ where L_x and L_y are the sizes of the computational domain.

The dispersion present in the numerical scheme is present in two forms, a purely dispersive piece, and a diffusive part, corresponding respectively to the real and imaginary parts of the dispersion relation $w(k)$ (w = frequency, k = wavenumber) for the difference scheme. The dispersion relation can easily be derived for a numerical scheme (such as used here) when it approximates a linear partial differential equation (PDE) such as

$$u_t + a\, u_x = b\, u_{xx}$$

where a and b are constants, with the usual results that the dispersion relation (both real and imaginary parts) for the numerical method matches the dispersion relation for the PDE to within reasonable accuracy for wavelengths longer than some minimum (fiducial) wavelength λ_{fld}. The value of λ_{fld} is dependent on the ratio a/b. For non-linear PDE's such as investigated here, the dispersion relation is not amenable to calculation and the results from linear analyses have to be assumed to hold locally and used as guidelines. For the second order accurate method employed here, investigations on the above PDE show such that $\lambda_{fld} \geq 5\, L_g$ to be an expected reasonable fiducial length for the parameter range discussed in this study.

The problem investigated here has, effectively, a smallest physical length scale determined by

$$R_{\min} = \min(R_{het}, R_{cap}) .$$

Care was taken to ensure that the relation

$$5\, R_g \leq R_{\min}$$

held for the calculations done here.† However, though due to computational memory/time limits, there are local areas in some of the calculations where $R_{cap} \geq 3R_g$. Some, isolated, local distortion of the calculation results (c.f. Fig. 8c), but does not affect the main conclusions of the calculation.

In addition to the above restrictions however, we find that if the length scale over which the heterogeneity varies, R_{het}, is less than the effective diffusion length scale, $\max(R_{disp}, R_{cap})$, the stability properties of the flow are the same as if the medium was homogeneous. (See § 4.2 .) This is a physical consequence of the diffusion term and reflects the enhanced stability emparted to the flow. This we propose is the main reason for failure of past efforts[6] to resolve the instability of immiscible flow numerically.

2. The Displacement Process

We consider the immiscible displacement determined by the following system,

$$\phi \frac{\partial S_i}{\partial t} + \nabla \cdot \mathbf{v}_i = 0 , \tag{1a}$$

$$\mathbf{v}_i = -\lambda_i(S_w)\, \nabla P_i , \qquad (i = o(il), w(ater)) ; \tag{1b}$$

where $S_w + S_o = 1$, and $\lambda_i = K(x, y)\, k_{ri}(S_i) / \mu_i$ is the mobility for component i. The rock permeability $K(x, y)$ is taken to be a scalar rather than a tensor field. Defining a mobility weighted average pressure

† The so-called 'grid orientation' problem is a well known example of the effects of numerical truncation error present in full scale reservoir simulators where the length scale of a grid block is almost always much larger than the smallest physical length scale associated with the problem. Indeed, for Buckley-Leverett or plug flows where the oil-water interface is effectively of zero width, numerical schemes must be employed which either have the same local dispersion characteristics as the partial differential equation being solved[10] or that have a dispersion characteristic which has controlled angular behaviour.[11]

stability of viscous fingering.

The problem can be characterized in terms of four dimensionless length scales:

1) $R_{cap} = L_{cap} / L$ characteristic of the capillary strength.

2) $R_{het} = L_{het} / L$ characteristic of either the heterogeneity in the medium (or characteristic of the length scale of perturbation(s) inserted in the initial data if the medium is homogeneous).

3) $R_g = L_g / L = \max(\Delta x, \Delta y) / L$ where Δx and Δy are the mesh spacings (assumed regular) of the grid.

4) $R_{disp} = L_{disp} / L$ characteristic of a minimum 'fiducial wavelength' for the numerical scheme due to inaccuracies arising from truncation error of the finite difference scheme employed.

In the above L is a reference length scale which we shall assume to be $L = \min(L_x, L_y)$ where L_x and L_y are the sizes of the computational domain.

The dispersion present in the numerical scheme is present in two forms, a purely dispersive piece, and a diffusive part, corresponding respectively to the real and imaginary parts of the dispersion relation $w(k)$ (w = frequency, k = wavenumber) for the difference scheme. The dispersion relation can easily be derived for a numerical scheme (such as used here) when it approximates a linear partial differential equation (PDE) such as

$$u_t + a\, u_x = b\, u_{xx}$$

where a and b are constants, with the usual results that the dispersion relation (both real and imaginary parts) for the numerical method matches the dispersion relation for the PDE to within reasonable accuracy for wavelengths longer than some minimum (fiducial) wavelength λ_{fid}. The value of λ_{fid} is dependent on the ratio a/b. For non-linear PDE's such as investigated here, the dispersion relation is not amenable to calculation and the results from linear analyses have to be assumed to hold locally and used as guidelines. For the second order accurate method employed here, investigations on the above PDE show such that $\lambda_{fid} \geq 5\, L_g$ to be an expected reasonable fiducial length for the parameter range discussed in this study.

The problem investigated here has, effectively, a smallest physical length scale determined by

$$R_{\min} = \min(R_{het}, R_{cap}) .$$

Care was taken to ensure that the relation

$$5\, R_g \leq R_{\min}$$

held for the calculations done here.[†] However, though due to computational memory/time limits, there are local areas in some of the calculations where $R_{cap} \geq 3R_g$. Some, isolated, local distortion of the calculation results (c.f. Fig. 8c), but does not affect the main conclusions of the calculation.

In addition to the above restrictions however, we find that if the length scale over which the heterogeneity varies, R_{het}, is less than the effective diffusion length scale, $\max(R_{disp}, R_{cap})$, the stability properties of the flow are the same as if the medium was homogeneous. (See § 4.2 .) This is a physical consequence of the diffusion term and reflects the enhanced stability emparted to the flow. This we propose is the main reason for failure of past efforts[6] to resolve the instability of immiscible flow numerically.

2. The Displacement Process

We consider the immiscible displacement determined by the following system,

$$\phi \frac{\partial S_i}{\partial t} + \nabla \cdot \mathbf{v}_i = 0 , \tag{1a}$$

$$\mathbf{v}_i = -\lambda_i(S_w)\, \nabla P_i , \qquad (i = o(il), w(ater)) ; \tag{1b}$$

where $S_w + S_o = 1$, and $\lambda_i = K(x, y)\, k_{ri}(S_i) / \mu_i$ is the mobility for component i. The rock permeability $K(x, y)$ is taken to be a scalar rather than a tensor field. Defining a mobility weighted average pressure

[†] The so-called 'grid orientation' problem is a well known example of the effects of numerical truncation error present in full scale reservoir simulators where the length scale of a grid block is almost always much larger than the smallest physical length scale associated with the problem. Indeed, for Buckley-Leverett or plug flows where the oil-water interface is effectively of zero width, numerical schemes must be employed which either have the same local dispersion characteristics as the partial differential equation being solved[10] or that have a dispersion characteristic which has controlled angular behaviour.[11]

$$P = \frac{(\lambda_w P_w + \lambda_o P_o)}{\lambda}, \tag{2}$$

where $\lambda = \lambda_w + \lambda_o$, and the capillary pressure

$$P_c = P_o - P_w, \tag{3}$$

system (1) can be written

$$\phi \frac{\partial S_w}{\partial t} + \nabla \cdot (f(S_w) \vec{v}) = \nabla \cdot (g(S_w) \nabla S_w), \tag{4a}$$

$$\nabla \cdot \vec{v} = 0, \tag{4b}$$

where

$$\vec{v} = -\lambda(S_w) \{ \nabla P + P_c(\vec{x}, S_w) f'(S_w) \nabla S_w \}, \tag{5}$$

$$f(S_w) = \frac{\lambda_w(S_w)}{\lambda(S_w)}, \tag{6}$$

$$g(S_w) = \frac{\lambda_w(S_w) \lambda_o(S_w)}{\lambda(S_w)} \left(-\frac{dP_c(S_w)}{ds} \right). \tag{7}$$

In (4), S_w and P are taken as the fundamental variables and P_c is assumed to be a known function of S_w and $\vec{x}$. The position dependence occurs in heterogeneous media. The mobility weighted average pressure (2) has the virtue over the unweighted average $(P_w + P_o) / 2$ of being finite for all S_w.

If $P_c(S_w) \equiv 0$, $P_w = P_o$, and (4) reduces to the familiar equations of Buckley-Leverett flow. However, (4) with $P_c \equiv 0$, is not a well-posed problem in the unstable flow regime; small wavelength disturbances grow at a rate inversely proportional to their wavelength. One must require physical dispersion (eg. capillarity) dominate over numerical dispersion to abtain a physically meaningful, well-posed problem.

3. The Numerical Approximation

Equation (4a) is degenerate parabolic; the effects of changes in saturation in one area propagate to surrounding areas with a finite speed. Equation (4b) is elliptic in the pressure P; all areas affect each other simultaneously - the propagation speed is infinite. Because of

the difference in time scales between these two equations, they can, with a great deal of confidence, be solved sequentially. One cycle consisting of solution of (4b) followed by (4a) shall be referred to as one iteration (or timestep). The main criterion for choice of the numerical scheme used to approximate (4a) and (4b) is that it introduce no numerical diffusion to mask the physical diffusion produced by the capillarity. This is achieved by approximating all derivatives by central differences.

With i, j and n denoting respectively the x, y and t indices, the numerical scheme used for (4a) consists of advection terms discretized by a leap-frog stencil, the viscosity term by a Crank-Nicholson stencil:

$$\frac{(S_{l,J}^{n+1} - S_{l,J}^{n-1})}{2\,\Delta t} + \frac{((\mathrm{v}\,f)_{l^+,J}^{n} - (\mathrm{v}\,f)_{l^-,J}^{n})}{\Delta x} + \frac{((\mathrm{v}\,f)_{l,J^+}^{n} - (\mathrm{v}\,f)_{l,J^-}^{n})}{\Delta y}$$

$$= \frac{1}{4\,\Delta x^2}\left\{g_{l^+,J}^{n}\,\Delta_x(u_{l^+,J}^{n+1} + u_{l^+,J}^{n-1}) + g_{l^-,J}^{n}\,\Delta_x(u_{l^-,J}^{n+1} + u_{l^-,J}^{n-1})\right\}$$

$$+ \frac{1}{4\,\Delta y^2}\left\{g_{l,J^+}^{n}\,\Delta_y(u_{l,J^+}^{n+1} + u_{l,J^+}^{n-1}) + g_{l,J^-}^{n}\,\Delta_y(u_{l,J^-}^{n+1} + u_{l,J^-}^{n-1})\right\}, \tag{8}$$

where

$$g_{l^+,J}^{n} = g\left(\frac{u_{l+1,J}^{n} + u_{l,J}^{n}}{2}\right),$$

$$g_{l^-,J}^{n} = g\left(\frac{u_{l,J}^{n} + u_{l-1,J}^{n}}{2}\right).$$

$$\Delta_x\,u_{l^+,J}^{n} = u_{l+1,J}^{n} - u_{l,J}^{n},$$

$$\Delta_x\,u_{l^-,J}^{n} = u_{l,J}^{n} - u_{l-1,J}^{n}. \tag{9}$$

Equation (4b) has the form

$$\nabla \cdot \lambda(S)\,\nabla P = \nabla \cdot h(S)\,\nabla S,$$

and was approximated by a Crank-Nicholson stencil:

$$\frac{1}{\Delta x^2}\left\{\lambda_{l^+,J}^{n}\,\Delta_x P_{l^+,J} - \lambda_{l^-,J}^{n}\,\Delta_x P_{l^-,J}\right\} + \frac{1}{\Delta y^2}\left\{\lambda_{l,J^+}^{n}\,\Delta_y P_{l,J^+} - \lambda_{l,J^-}^{n}\,\Delta_y P_{l,J^-}\right\}$$

$$= \frac{1}{\Delta x^2}\left\{h_{l^+,J}^{n}\,\Delta_x S_{l^+,J}^{n} - h_{l^-,J}^{n}\,\Delta_x S_{l^-,J}^{n}\right\} + \frac{1}{\Delta y^2}\left\{h_{l,J^+}^{n}\,\Delta_y S_{l,J^+}^{n} - h_{l,J^-}^{n}\,\Delta_y S_{l,J^-}^{n}\right\} \tag{10}$$

The difference scheme is second order accurate in space and time. The linear system of equations generated on the numerical grid for each equation at each timestep were inverted using a multigrid algorithm[12] of relaxation and injection through a sequence of coarser grids which is based on a variational formulation of the equations (4).

The calculations were performed in a square, length L, width L. The boundary conditions imposed were (S is defined in (11))

$$\begin{aligned} S &= 1\,, \quad \text{at } y = 0\,, \qquad S = 0\,, \quad \text{at } y = L\,, \\ \frac{\partial S}{\partial x} &= 0 \qquad \text{at } x = 0, L\,, \\ P &= P_0, \quad \text{at } y = 0, \qquad P = 0, \quad \text{at } y = L\,, \\ \frac{\partial P}{\partial x} &= 0 \qquad \text{at } x = 0, L\,, \\ u(x, y, t = 0) &= u_0(x, y)\,. \end{aligned} \tag{11}$$

The calculation neglects the initial displacement flow into the block during which the water saturation at $y = 0$ rises from S_{wc} to $1 - S_{orw}$. It is not expected that the initial flow into the block will affect the stability properties of the displacement and hence this initial transient flow is neglected. Further, this choice simplifies the saturation boundary condition.

The constant pressure drop boundary condition contrasts with the (perhaps more common) experimental condition of maintaining constant flow rate. Constant flow rate calculations can be included but are more complicated due to the non-uniform flow at $y = 0$. Again, the stability properties of the system are not expected to be qualitatively different for the two types of boundary conditions.

4. Analysis of Case Studies

In the absence of capillarity, the Buckley-Leverett mixing zone terminates in a sharp oil-water interface, with a unique water saturation S_w^* just behind the front. If S_{wc} denotes the connate water saturation ahead of the front, the frontal mobility ratio,

$$M^* = \frac{\lambda(S_w^*)}{\lambda(S_{wc})} \tag{12}$$

is a measure of the potential instability of the front to viscous fingering. The 'far field' mobility ratio,

$$M = \frac{\lambda(1 - S_{orw})}{\lambda(S_{wc})}, \tag{13}$$

is a measure of the potential instability of the front only in the case of two regions of one-phase flow, i.e., plug flow. The importance of M and M^* is verified by linearized stability analyses of plug flow and of Buckley-Leverett flow. Although genuine two-phase flow is usually encountered, M is commonly used instead of M^* as an index of instability because it is more easily measured in routine laboratory work. In general, $M > M^*$, and thus there is a region of parameter space for which M^* indicates stability while M indicates instability.

When capillary forces are included, the sharp oil-water front disappears, replaced by a region of smooth rarefaction from S^* to S_{wc} over a length scale L_{cap} characteristic of the local capillary strength. The mixing zone is thus increased over the Buckley-Leverett case, and the system is expected to have further enhanced stability against viscous fingering. As L_{cap} increases, both M and M^* become poorer indicators for the stability of the displacement. Assuming quadratic permeability functions,

$$k_{rw} = k_{wm} S^2, \qquad k_{ro} = k_{om} (1 - S)^2, \tag{14}$$

where

$$S = \frac{S_w - S_{wc}}{1 - S_{orw} - S_{wc}}, \tag{15}$$

the far-field and frontal mobility ratios for Buckley-Leverett flow are given by

$$M = \frac{\mu_o}{\mu_w} \frac{k_{wm}}{k_{om}}, \tag{16}$$

$$M^* = 2\left(1 - (1 + M)^{-1/2}\right). \tag{17}$$

From (16) and (17), $0 \le M < \infty$ whereas $0 \le M^* < 2$, reflecting the increased stability of immiscible flow.

It is expected[13,14] that a variety of factors affect the stability properties of two phase, immiscible, incompressible displacement. These include

- mobility ratio of the fluids present
- strength of capillary forces
- size of existing perturbations in the flow
- heterogeneity of the reservoir
- injection rate of displacing fluid
- presence of injection and production wells.

The first four factors are examined in this study. Because of our boundary conditions the last two were not studied.

As it is computationally impractical to pursue a full mapping of the parameter space, our calculations present projections of the 'stability manifold' along a portion of each of the parameter axes studied and show the development towards instability for each.

All computations were performed in a square (in the x, y plane) slice of rock of porosity 0.18 and average rock permeability K = 106 mD.

The pressure drop maintained across the block (in the y direction) is such that if the slice had a cross-sectional area of 15.9 cm (in the x, z plane), the flow rate would be 0.00398 cm^3 / sec. at $t = 0$. The relative permeability functions were modelled by the quadratic forms (14), and the capillary function represented by

$$P_c = P_0(x, y) \ln S \quad \text{(atm)} . \tag{18}$$

These functions and constants are characteristic of sandstone.[15]

Two measurements were used in analysing perturbation (finger) growth. Figure 1 illustrates the measurement of the height (H) and full width at half maximum (FWHM) for a finger present in a particular saturation contour $S = S_{ct}$ at some time $t \geq 0$ in the flow. Stability of a contour level is examined by plotting H and the ratio H / FWHM for a finger as a function of time. In all cases only the contours S = 0.8, 0.6, 0.4, 0.2, 0.0 were analyzed.

4.1. Homogeneous Rock Studies

For homogeneous rock, ($K(x, y)$ = const, $P_0(x, y)$ = const) the initial data $u_0(x, y)$ consisted of a finger, imposed on a one-dimensional-flow profile $\bar{u}_0(y)$. While the one dimensional profile could have been obtained from one dimensional calculations for which the water saturation at $y = 0$ builds up from S_{wc} to $1 - S_{orw}$, we chose instead to initialize $\bar{u}_0(y)$ with a quadratic shape. (See Fig. 2c .) This also simplified the choice of how to impose the fingered perturbation; it was given a quadratic variation in x, y. (See Fig. 2a .) Consequently, our calculation includes some initial transients as the flow adjusts. We emphasize again, that these transients are not expected to significantly affect the stability properties of the displacement process; to whit: if a certain choice of parameters in our calculation indicates an instability of a certain growth rate, the instability with the same growth rate results whether or not the transients are included. Figure 2 displays a selection of plots showing the perturbation development for a particular run (run 3 of §4.1.3). Shown is the saturation development for four equally spaced timesteps (Fig. 2a), the final pressure, saturation and velocity fields in the run (Fig. 2b), and the cross sectional pressure and saturation profiles along the mid-line $x / L = 0.5$ for 5 equally spaced timesteps (Fig. 2c) . From finger growth measurements, the perturbation shown here is seen to be slightly unstable.

4.1.1. Stability Dependence on Mobility Ratio

A moderately large finger was initialized on a one dimensional background flow. For the S = 0.8, 0.6, 0.4, 0.2, 0.0 contours, the size of the perturbation introduced is given below.

sat	H / L	FWHM / L
0.8	0.15	0.23
0.6	0.21	0.23
0.4	0.26	0.23
0.2	0.30	0.23
0.0	0.32	0.23

Measurements of the finger development on these contours were taken at constant time intervals during the run for three different mobility ratios:

run	M^*	M
1	0.722	1.45
2	1.0	3.0
3	1.397	10.0

In all cases the mobility ratio was determined by choosing $\mu_w = 1$, $\mu_o = 10$, $k_{om} = 1$ and varying k_{wm} appropriately. The capillary force was set by using $P_0 = 0.005$ atm. giving a measured capillary length scale $R_{cap} \approx 0.05$.

The results of finger height versus injected pore volume for the analyzed contours are presented in Fig. 3a. As expected, the flow is much more unstable for run 3 than for run 1 . All contour levels analyzed are unstable for runs 2 and 3, whereas only the 0.8 and 0.6 contours are unstable in run 1.† We note that the growth rate of the height (after initial transients have disappeared) is, to a first approximation, linear. This is in accord with results obtained for large scale perturbations in Buckley-Leverett flow.[13]

Fig. 3b plots the ratio H / FWHM versus injected pore volume for the same three runs.

4.1.2. Stability Dependence on Initial Finger Size

In a second series of calculations, the mobility ratio and capillary pressure constant were held constant at $M^* = 1.397$, $P_0 = 0.005$ ($R_{cap} \approx 0.05$) and the size of the perturbation in the initial data varied. For the $S = 0$ contour, the initial perturbation sizes were†

run	H / *L*	FWHM / *L*
1	0.09	0.07
2	0.19	0.14
3	0.32	0.23
4	0.54	0.23

The results are plotted in Fig. 4a and b. The flow becomes more stable as the initial

† There is some question as to whether the initial transient flow for the 0.8 and 0.6 saturation contours has terminated in this run or whether it is still adjusting from the initial conditions. These contours are initially isolated from the frontal flow and in flows of borderline stability can be expected to remain thus isolated for a longer period of time.

† The heights given in column two of the table are numerical approximations to 0.1, 0.2, 0.33 and 0.55 which arise due to the finite size of the grid spacing.

perturbation size decreases.

4.1.3. Stability Dependence on Capillary Pressure

For a third series of runs, the mobility ratio and initial perturbation size were held constant ($M^* = 1.397$, initial perturbation as in Fig. 3) and the capillary pressure constant P_0 varied:

run	P_0
1	0.005
2	0.01
3	0.02
4	0.05
5	0.1

The results are shown in Fig. 5. Sufficient increase in capillarity is seen to stabilize the flow.

4.1.4. Comparison with No Capillarity

The front tracking code of Glimm, McBryan, et. al.,[10] was used to provide a comparison to instability growth for the case of zero capillarity (Buckley-Leverett) flow. For these calculations, a finger was initialized in a homogeneous medium such that the contour level S^* at $t = 0$ occurred at the same position as it would in a run with capillarity. The same quadratic saturation profile behind the S^* contour (now the oil-water front) was initialized as occured in the case with capillarity. Fig. 6a displays H and FWHM as a function of time for the $S^* = 0.5$ contour for such a run with $M^* = 1$. It is superimposed upon the analogous plots for the $S = 0.0, 0.2, 0.4, 0.6, 0.8$ contours of a run with capillarity $P_0 = 0.005$. Fig. 6b shows the same superposition for $M^* = 1.397$. The effect of capillarity is found to affect the rate of growth of finger height much more strongly than the FWHM.

4.2. Studies in Heterogeneous Rock

The heterogeneity properties of reservoir rock vary according to rock type. We employ here a characterization of heterogeneity in terms of a length scale and a variance of the rock properties over this length scale. The rock heterogeneity is given by a random variable

(field) $K(x, y) = K_{av}\,\chi(x, y)$ which has a given variance about the mean K_{av} over a length scale L_{het}. A 'heterogeneity mesh' $\Delta x = \Delta y = L_{het}$ is superimposed on the computational square. Uniformly distributed numbers are determined at the nodes of this mesh. Each uniformly distributed number is then converted to a normally distributed number. These are then interpolated into each mesh square to obtain a random field at any computational point. Fig. 7 presents a plot of the heterogeneity field produced for $L_{het} = 0.05$. (The numbers displayed in the plot are relative.) It has the subjective disadvantage of 'not looking very heterogeneous', especially for larger R_{het} values (Compare Figures 7 and 9b), largely due to the underlying regular grid structure and linear interpolation by which it is constructed. This formulation does however isolate a single length scale for the heterogeneity. In contrast to real rock though, any interactions due to interplay between different length scales of heterogeneity are absent.

The variation of capillary pressure with the now spatially dependent rock permeability is taken into account using the Leverett 'J'-function analysis. Consequently, for the studies in heterogeneous rock $P_0(x, y)$ in (18) becomes

$$P_0(x, y) = \frac{P_{av}}{(\chi(x, y))^{1/2}} \quad . \tag{19}$$

where P_{av} is a constant.

A series of calculations were made for a displacement flow of given frontal mobility ratio and capillary pressure over media of varying heterogeneity length scale for constant heterogeneity variance. The saturation profile was initialized as a one dimensional flow $u_0(x, y) = \tilde{u}_0(y)$ with a quadratic variation in the y direction. Three runs were made for with $M^* = 1.397$, $P_{av} = 0.005$, with a very strong variance in the heterogeneity (permeability varying by a factor of 400).

run	L_{het} / L
1	0.02
2	0.05
3	0.20

Figures 8a plots the saturation versus injected pore volume at four equally spaced time intervals for run 1. Figures 8b and 8c present the corresponding plots for runs 2 and 3. In Fig. 8a the capillary length scale is approximately twice as large as the heterogeneity length scale. *In spite of the strong variation in the heterogeneity, the flow is stable, the variation of a saturation contour does not grow with time.* In Fig. 8b the heterogeneity and capillary length scales are approximately equal. In Fig. 8c, the flow is cleary unstable; pockets of oil are being trapped in low mobility regions as neighbouring fingers flow around the region and entrap. In Fig. 9a we present the results for a run with a much smaller range of variation variation in the heterogeneity. For this run $R_{\ell} = 0.0077$, $R_{cap} \geq 0.03$, $R_{het}=0.3$. and the heterogeneity (Fig. 9b) in the permeability varies by a maximum of 4.3 . The flow is still clearly unstable.

5. Conclusions

We have presented numerical calculations that are in good qualitative agreement with laboratory studies indicating fingering phenomenon for immiscible flow in reservoir rock samples. Our calcualtions show that, although immiscible displacement is expected to be much more stable than miscible, it is none-the-less significantly unstable with respect to viscous fingering over a large range of its parameter space. Calculations in homogeneous rock show that mobility ratio, capillary pressure, and perturbation size are factors that control the instability of the flow. While growth of small perturbations is largely driven by the frontal mobility ratio, the growth of large perturbations cannot in general be characterized by a single mobility ratio, though the frontal mobility ratio tends to be a better indicator than the far field mobility ratio. Both unstable growth and stable decay of finger height are found to be well characterized by constant rates.

The introduction of heterogeneity in the medium leads to the evolution of finger patterns with the proviso that fingers induced by heterogeneity on length scales small compared to the capillary length are strongly damped by capillarity; the medium appears effectivley homogeneous over these small length scales. Where the heterogeneity length scale exceeds the capillary length scale, the displacement flow 'sees' significant mobility channels which will act as nucleation points for perturbations in the displacement flow. The subsequent growth rate of these perturbations must then depend upon the size of the perturbation achieved as a

result of the channel and the mobility ratio of the fluids involved.

Comparison with runs with no capillarity show the expected results that capillarity tends to broaden existing fingers and enhance the stability of the flow.

Nomenclature

i = phase, w(ater) or o(il)

k_{ri} = relative permeability, phase i

k_{om} = maximum oil relative permeability ($S = 0$)

k_{wm} = maximum water relative permeability ($S = 1$)

K = rock permeability

λ_w = water mobility

λ_o = oil mobility

λ = total fluid mobility

L = computational region length scale

L_{cap} = capillary length scale

M = 'far field' mobility ratio

L_{het} = heterogeneity length scale

M^* = frontal mobility ratio defined for Buckley-Leverett flow

μ = viscosity

o = oil

P_o = oil pressure

P_w = water pressure

P = mobility weighted average pressure

P_c = capillary pressure

S_o = oil saturation

S_w = water saturation

S_{wc} = connate water saturation

S_{orw} = residual oil saturation

S = normalized water saturation ($0 \leq S \leq 1$)

v = total fluid velocity

v_o = oil velocity

v_w = water velocity

w = water

χ = heterogeneity random variable

References

1. R. L. Chouke, P. van Meurs, and C. van der Poel, "The Instability of Slow, Immiscible Viscous Liquid-Liquid Displacement in Permeable Media.," *Trans. AIME*, vol. 216, pp. 188-194, 1959.

2. F. J. Fayers, "An Approximate Model with Physical Interpretable Parameters for Representing Miscible Viscous Fingering," *SPE 13166*, 1984.

3. S. Vossoughi, J. E. Smith, D. W. Green, and G. P. Willhite, "A New Method to Simulate the Effects of Viscous Fingering on Miscible Displacement Processes in Porous Media," *Soc. Pet. Eng. J.*, vol. 24, pp. 56-64, 1984.

4. E. J. Koval, "A Method for Predicting the Performance of Unstable Miscible Displacement in Heterogeneous Media," *Soc. Pet. Eng. J.*, vol. 3, pp. 145-154, 1963.

5. R. E. Ewing, T. F. Russell, and M. F. Wheeler, "Simulation of Miscible Displacement Using Mixed Methods and a Modified Method of Characteristics," *SPE 12241*, 1983.

6. H. H. Rachford, "Instability in Water Flooding Oil from Water-Wet Porous Media Containing Connate Water," *Trans., AIME*, vol. 231, pp. 133-148, 1964.

7. S. T. Lee, K. M. G. Li, and W. E. Culham, "Stability Analysis of Miscible Displacement Processes," *SPE/DOE 12631*, 1984.

8. G. R. Jerauld, H. T. Davis, and L. E. Scriven, "Stability of Fronts of Permanent Form in Immiscible Displacement," *SPE 13164*, Sept. 1984.

9. E. J. Peters and D. L. Flock, "The Onset of Instability During Two-Phase Immiscible Displacement in Porous Media," *SPE 8371*, 1979.

10. J. Glimm, E. Isaacson, D. Marchesin, and O. Mcbryan, "Front Tracking for Hyperbolic Systems," *Adv. in Appl. Math.*, vol. 2, pp. 91-119, 1981.

11. G.R. Shubin and J.B. Bell, "An Analysis of the Grid Orientation Effect in Numerical Simulation of Miscible Displacement," *Computer Methods in Appl. Mech. and Engin. (to appear).*

12. J. Goodman, R. Kohn, and L. Reyna, *In preparation.*.

13. J. Glimm, E. Isaacson, B. Lindquist, O. McBryan, and S. Yaniv, "Statistical Fluid Dynamics II: The Influence of Geometry on Surface Instabilities," in *Frontiers in Applied Mathematics*, vol. 1, SIAM, Philadelphia, 1983.

14. A. J. Chorin, "The Instability of Fronts in a Porous Medium," *Comm. Math. Phys.*, vol. 91, pp. 103-116, 1983.

15. F. R. Allen, G. P. Maddison, and D. A. Puckett, "Theoretical and Experimental Studies of Rate Dependent Two-Phase Immiscible Flow," *SPE 10972*, Sept. 1982.

Figure Captions

Fig. 1 A sketch of a finger illustrating the measurement of finger height and full width at half maximum (FWHM).

Fig. 2 a) Contours of saturation at four equally spaced timesteps for run 3 of §4.1.3 . b) Contours of pressure (upper left hand corner), saturation (upper right) and velocity magnitude (lower) for the final timestep of run 3 of §4.1.3 . c) Cross sectional profiles along the mid-line $x = 0.5$ of the pressure (upper graph) and saturation (lower graph) for 5 equally spaced timesteps.

Fig. 3 a) Finger height versus injected pore volume for three mobility runs in homogeneous rock: left to right $M^* = 0.722, 1.0, 1.397$. For each run the contours $S = 0.8, 0.6, 0.4, 0.2, 0.0$ are represented (respectively, from the bottom to top at $t = 0$). Plot lines that terminate early in time indicate the contour line reaches $y = L$ shortly thereafter. The vertical and horizontal scales are the same for all three runs. b) The ratio H / FWHM versus injected pore volume. All other comments in a) apply.

Fig. 4 a) Finger height versus injected pore volume for four choices of initial perturbation size corresponding (left to right) respectively to the runs 1 through 4 described in §4.1.2 . For each run the contours $S = 0.8, 0.6, 0.4, 0.2, 0.0$ are represented (respectively, from the bottom to top at $t = 0$). Plot lines that terminate early in time indicate the contour line reaches $y = L$ shortly thereafter. The vertical and horizontal scales are the same for all three runs. b) The ratio H / FWHM versus injected pore volume. All other comments in a) apply.

Fig. 5 a) Finger height versus injected pore volume for five choices of capillary pressure strength left to right $P_0 = 0.005, 0.01, 0.02, 0.05, 0.1$ atm. For each run the contours $S = 0.8, 0.6, 0.4, 0.2, 0.0$ are represented (respectively, from the bottom to top at $t = 0$). Plot lines that terminate early in time indicate the contour line reaches $y = L$ shortly thereafter. The vertical and horizontal scales are the same for all three runs. b) The ratio H / FWHM versus injected pore volume. All other comments in a) apply.

Fig. 6 a) Comparison of height and FWHM versus injected pore volume for the S_* contour in a run with no capillarity with the analyzed contours for a corresponding run with $P_0 = 0.005$. The frontal mobility ratio is 1.0 . b) As in a) with a frontal mobility ratio of 1.397 .

Fig. 7 The heterogeneity field (contours of constant heterogeneity) with a length scale $L_{het} / L = 0.05$, variance = 1.0 .

Fig. 8 a) The saturation $S(x, y)$ at four equally spaced timesteps for run 1 of § 4.2 . b) The saturation $S(x, y)$ at four equally spaced timesteps for run 2 of § 4.2 . c) The saturation $S(x, y)$ at four equally spaced timesteps for run 3 of § 4.2 . A small amount of numerical instability has produced small oscillation behaviour in the trapped oil regions.

Fig. 9 a) The saturation $S(x, y)$ at four equally spaced timesteps for the final run discussed in § 4.2 . b) The heterogeneity function $\chi(x, y)$ for this run.

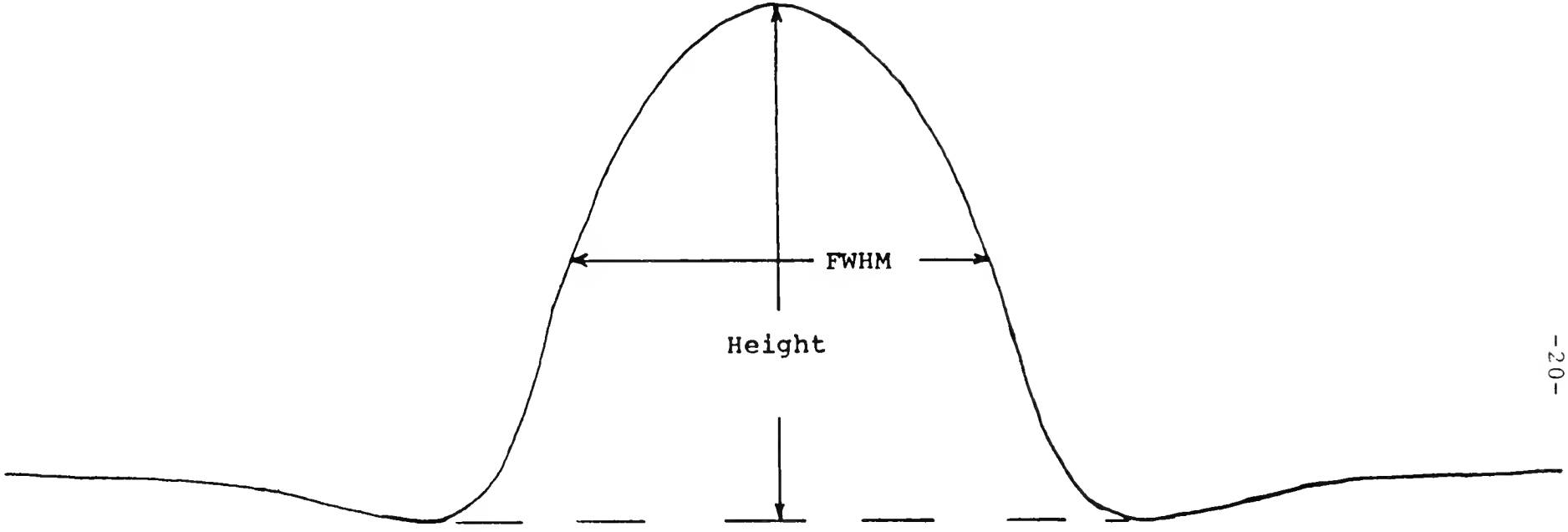

Fig. 1

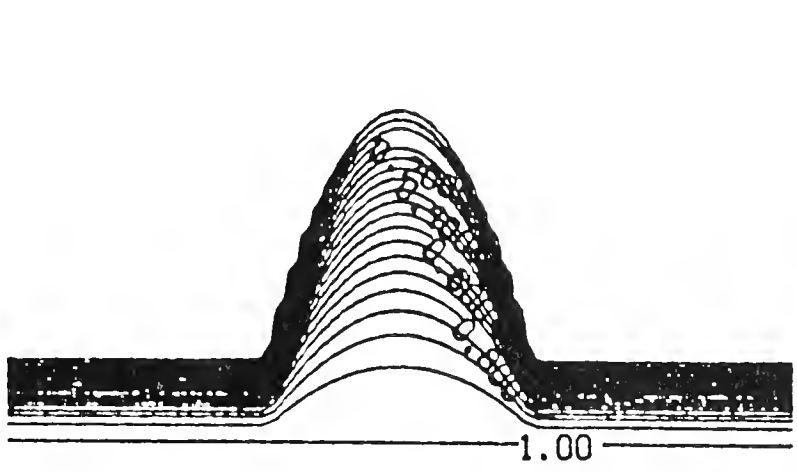

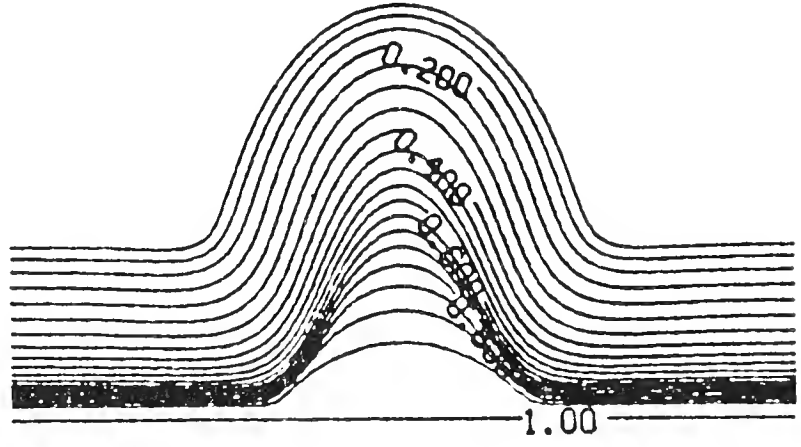

Fig. 2a

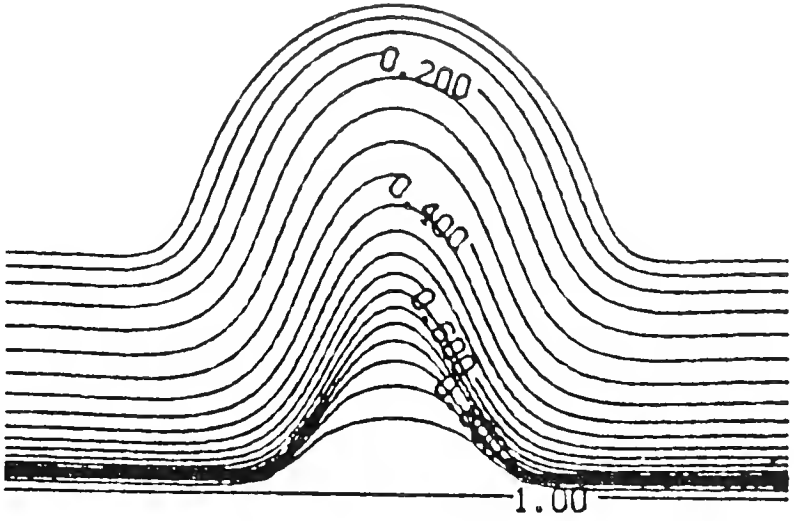

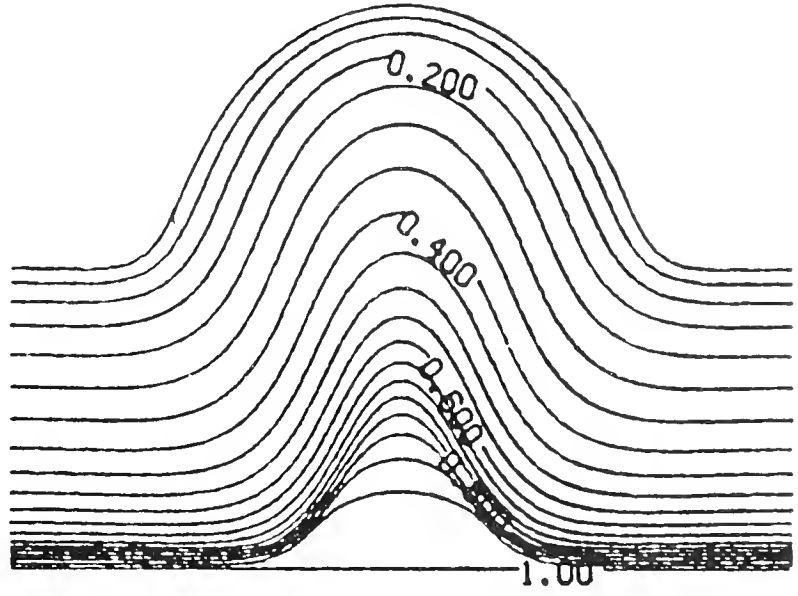

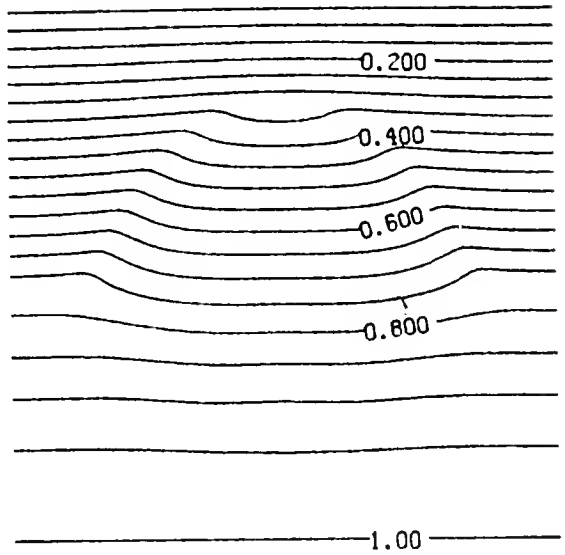

Pressure

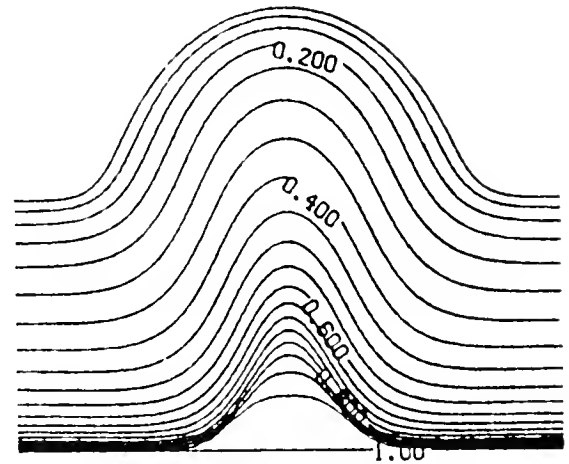

Saturation

Fig. 2b

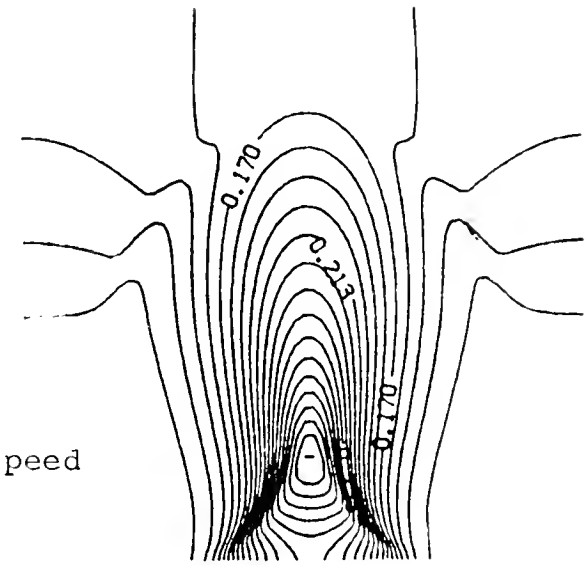

Speed

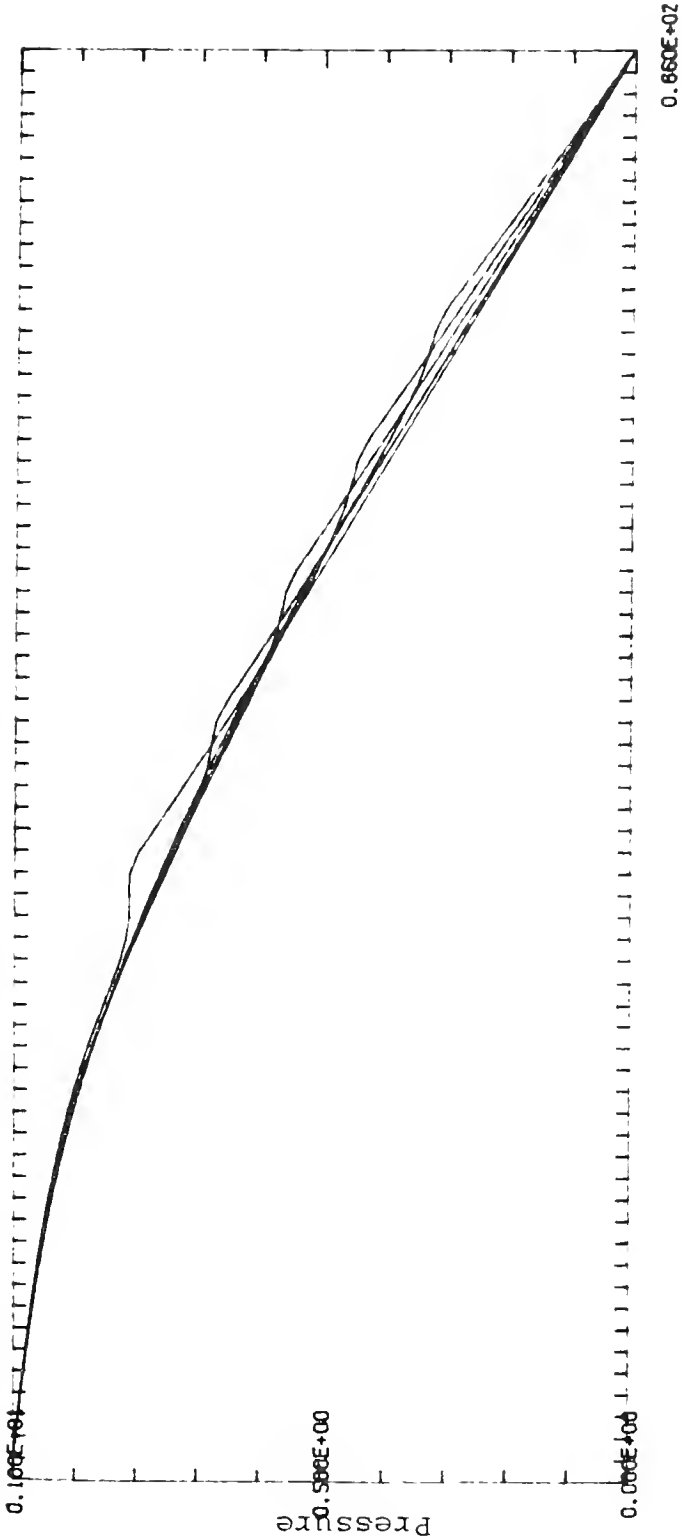
Pressure
0.100E+01
0.500E+00
0.000E+00
0.860E+02

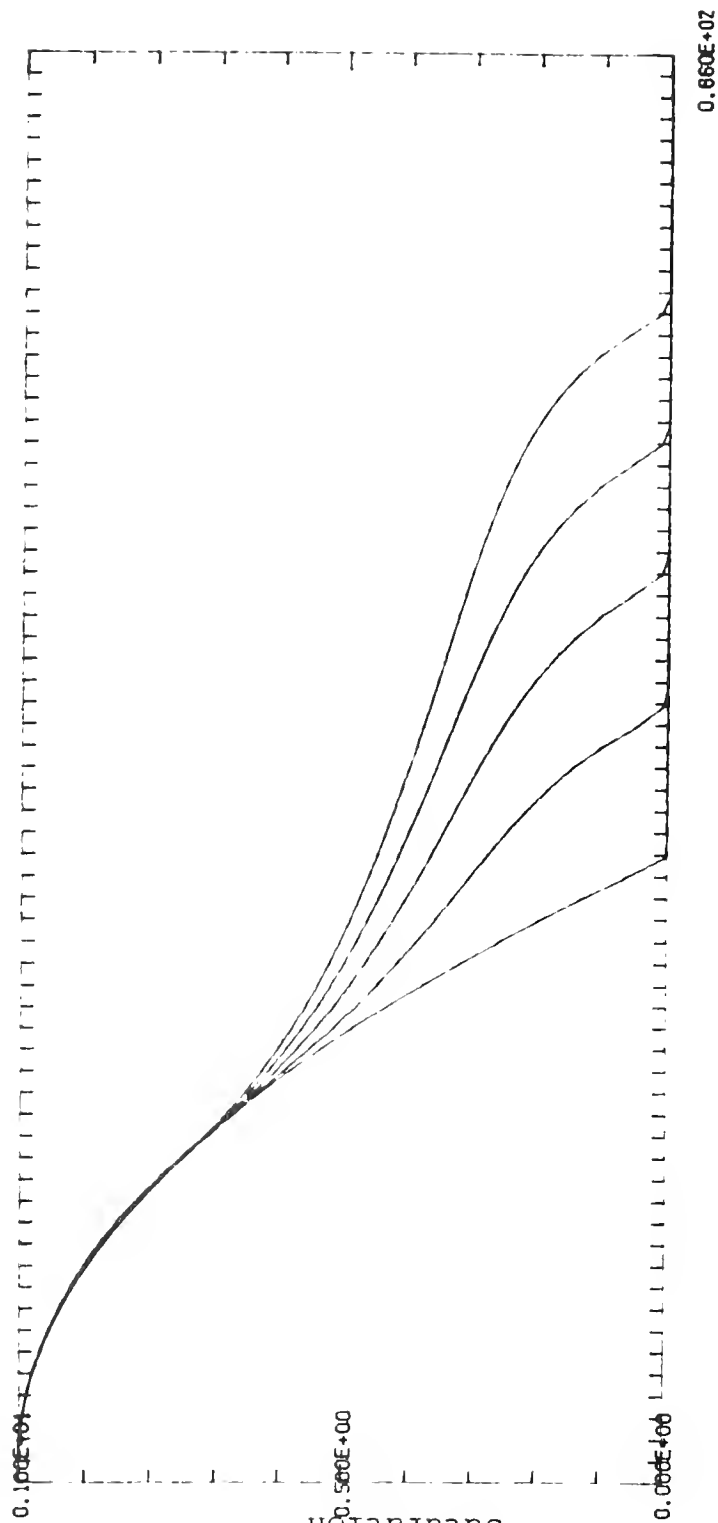
Saturation
0.100E+01
0.500E+00
0.000E+00
0.860E+02

Fig. 2c

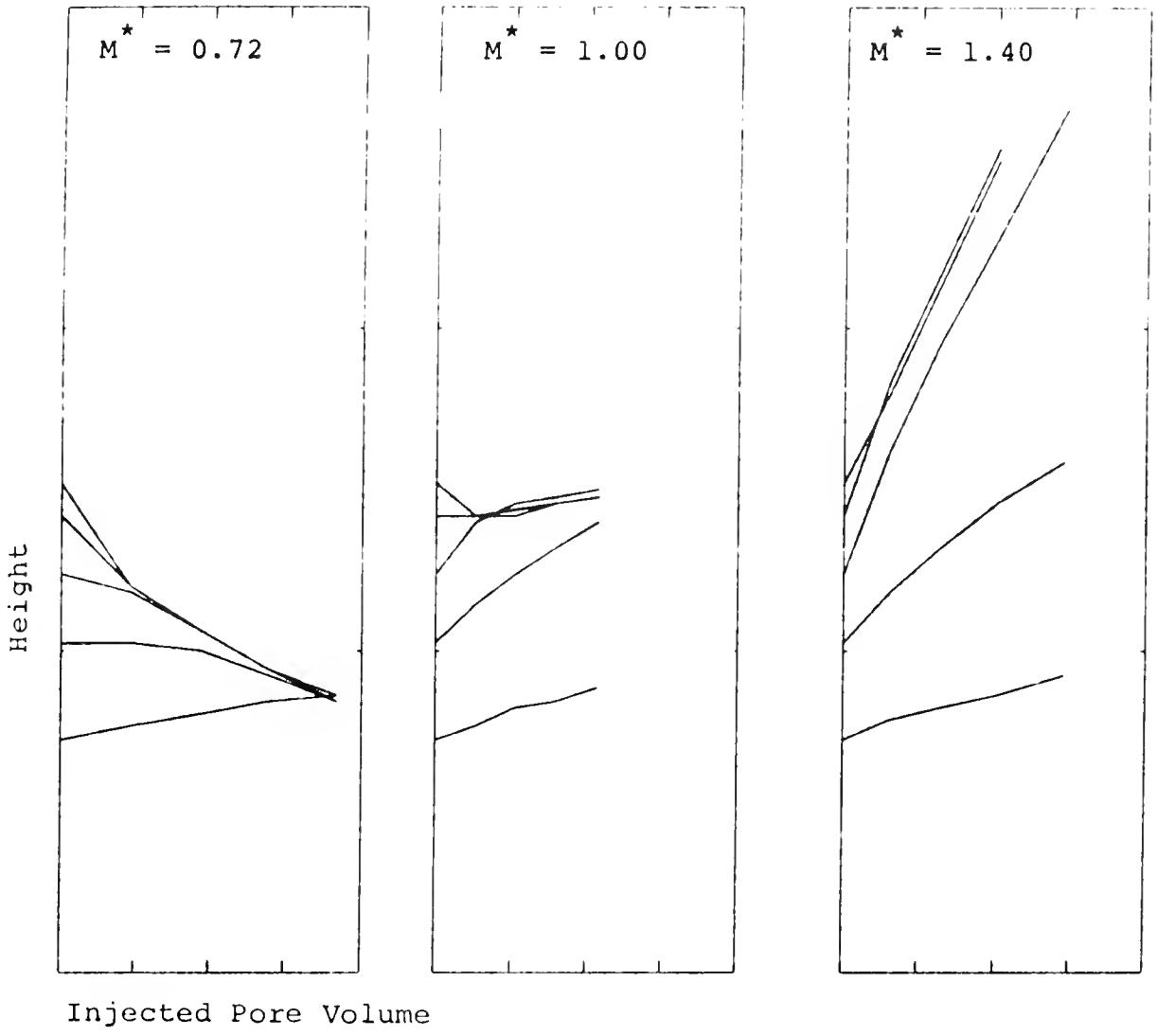

Fig. 3a

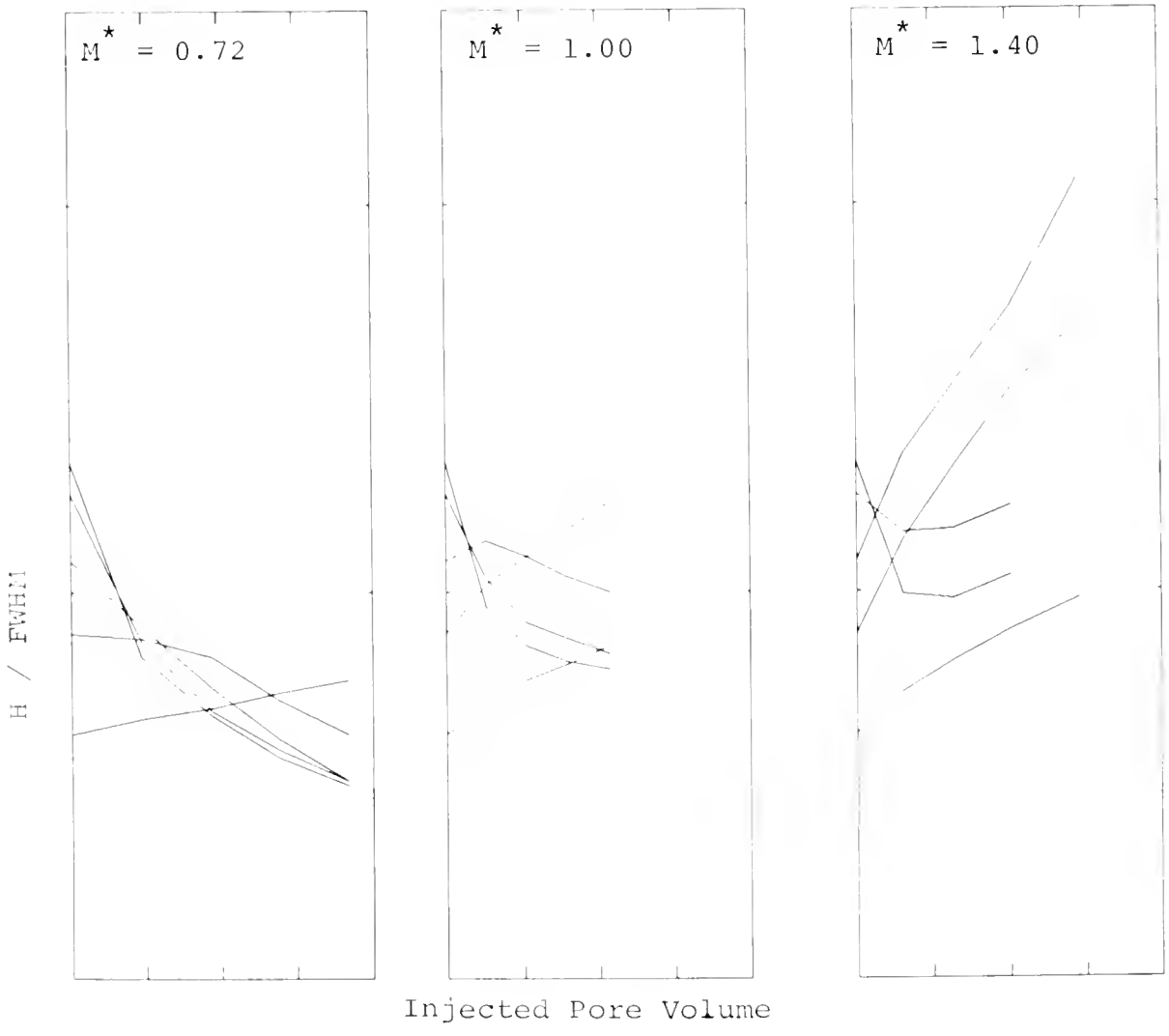

Fig. 3b

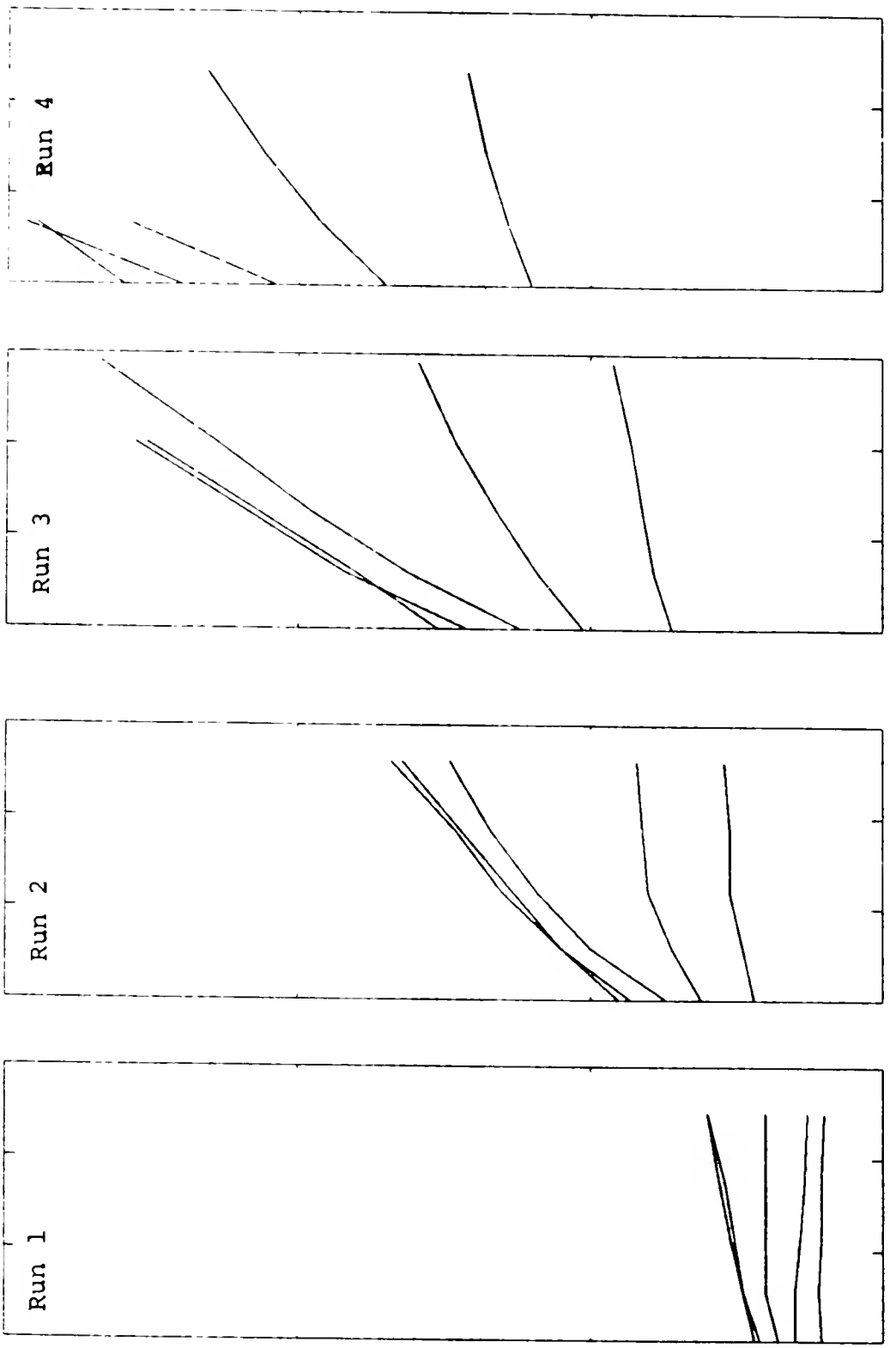

Fig. 4a

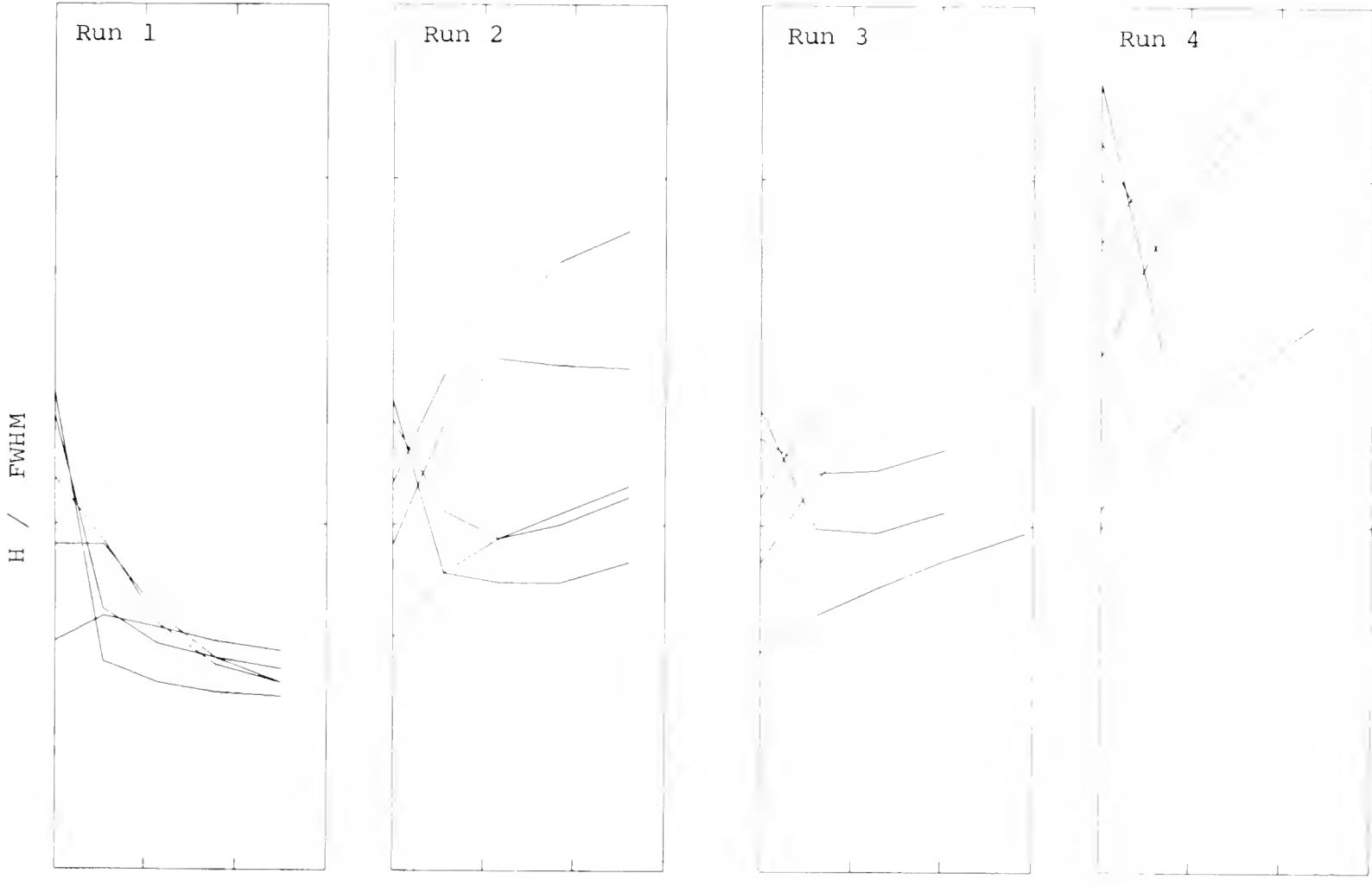

Fig. 4b

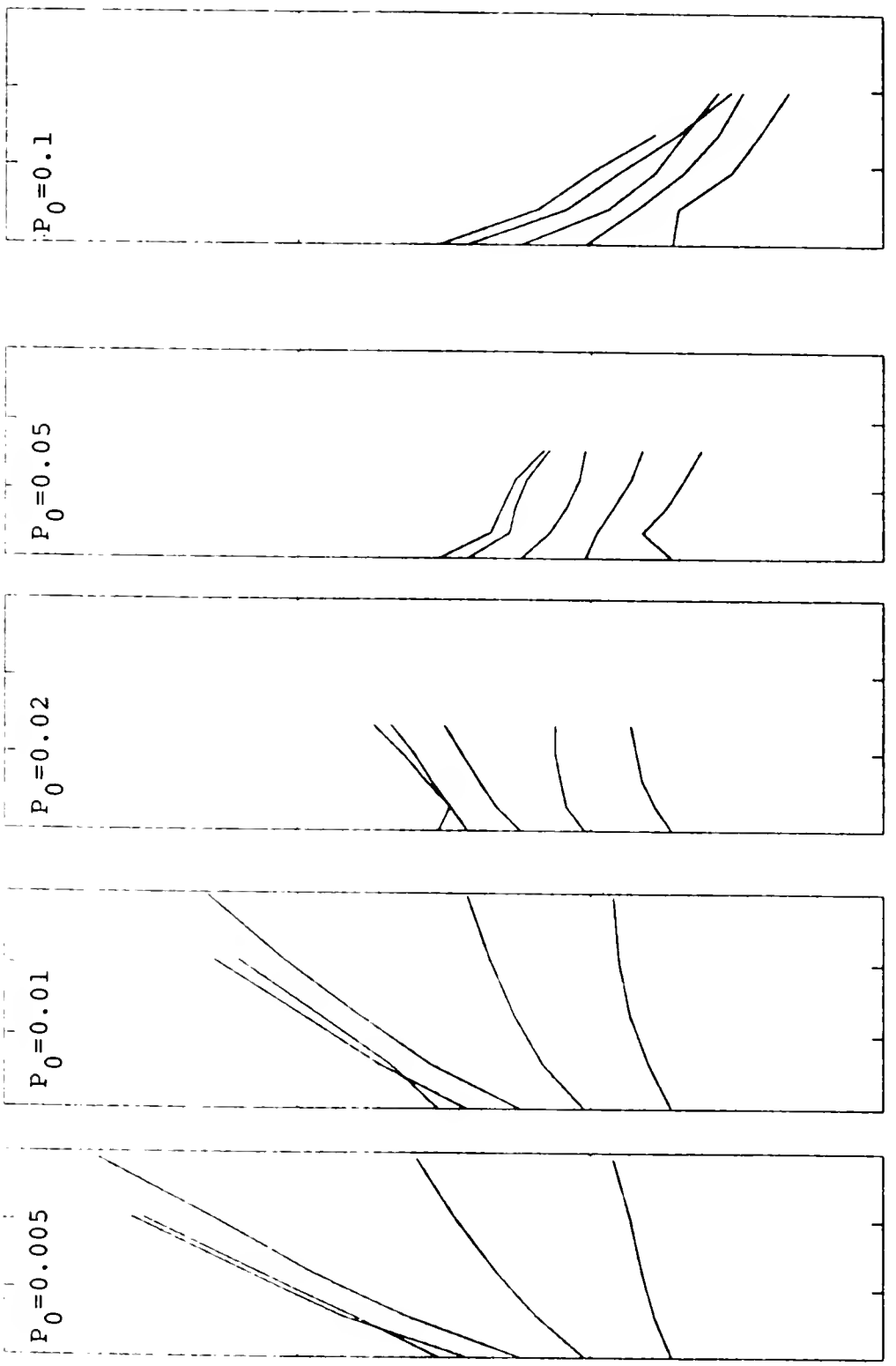

Fig. 5a

Fig. 5b

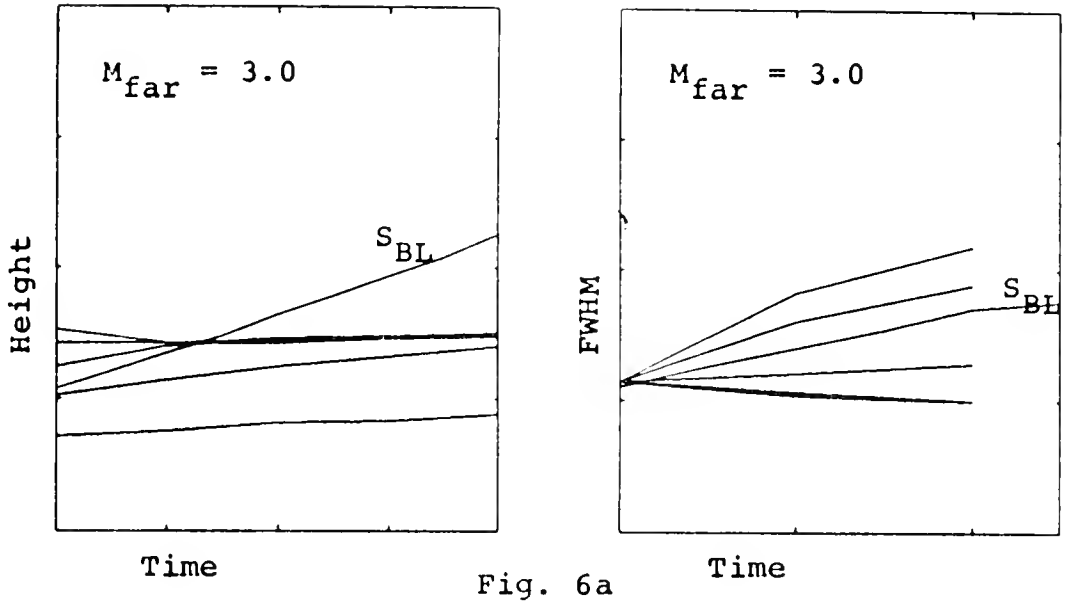
M_{far} = 3.0
S_{BL}
Height
Time
M_{far} = 3.0
S_{BL}
FWHM
Time

Fig. 6a

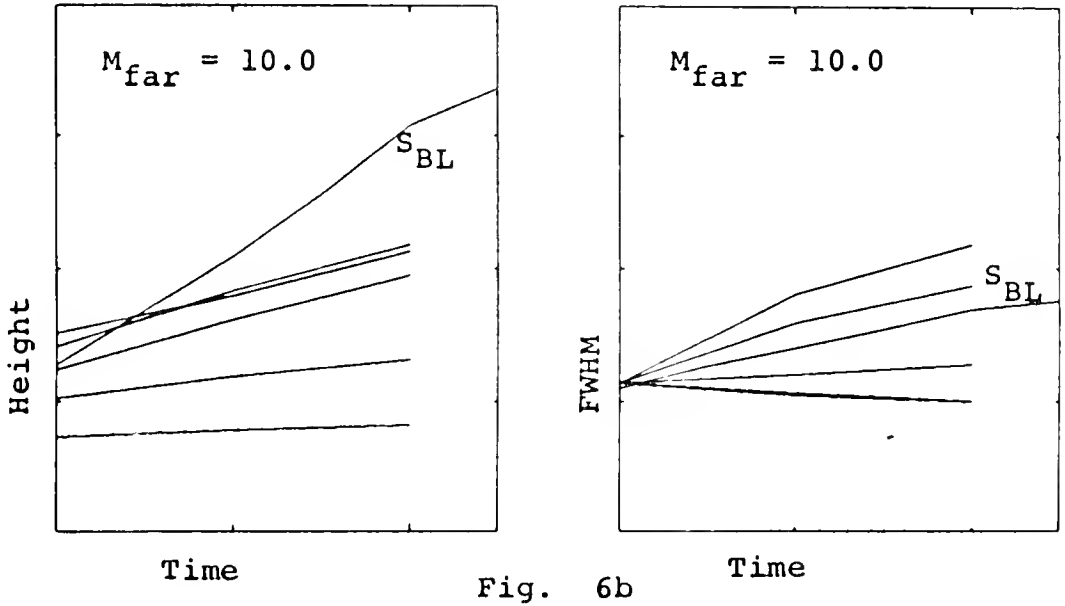
M_{far} = 10.0
S_{BL}
Height
Time
M_{far} = 10.0
S_{BL}
FWHM
Time

Fig. 6b

Fig. 7

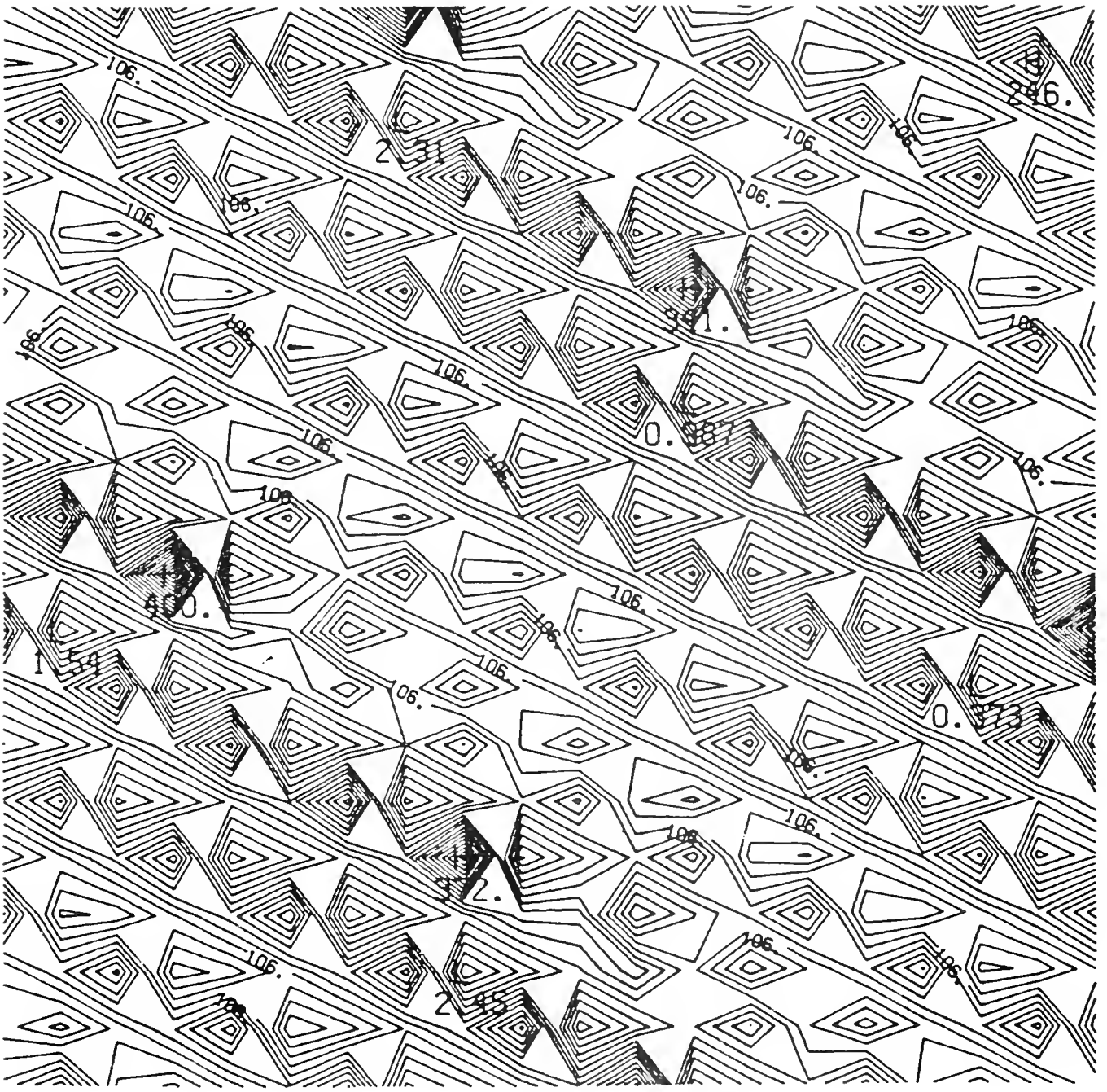
106.
106.
106.

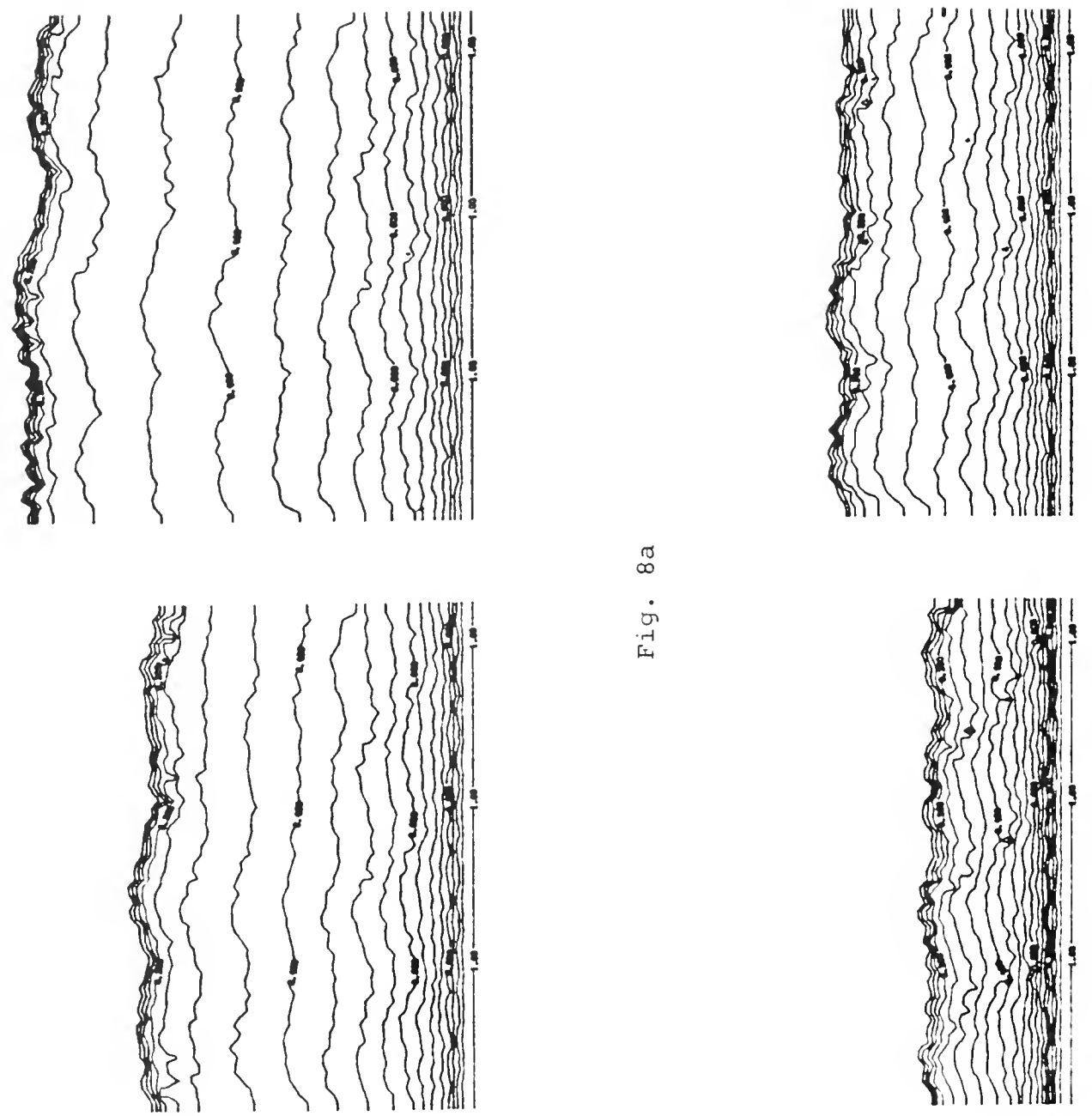

Fig. 8a

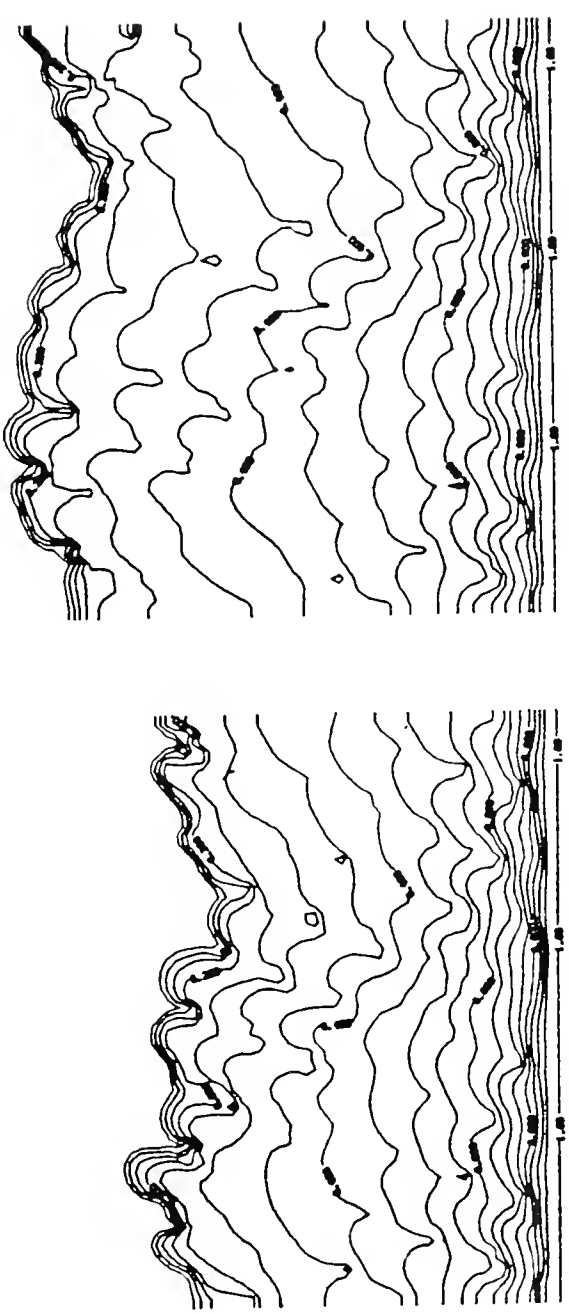

Fig. 8b

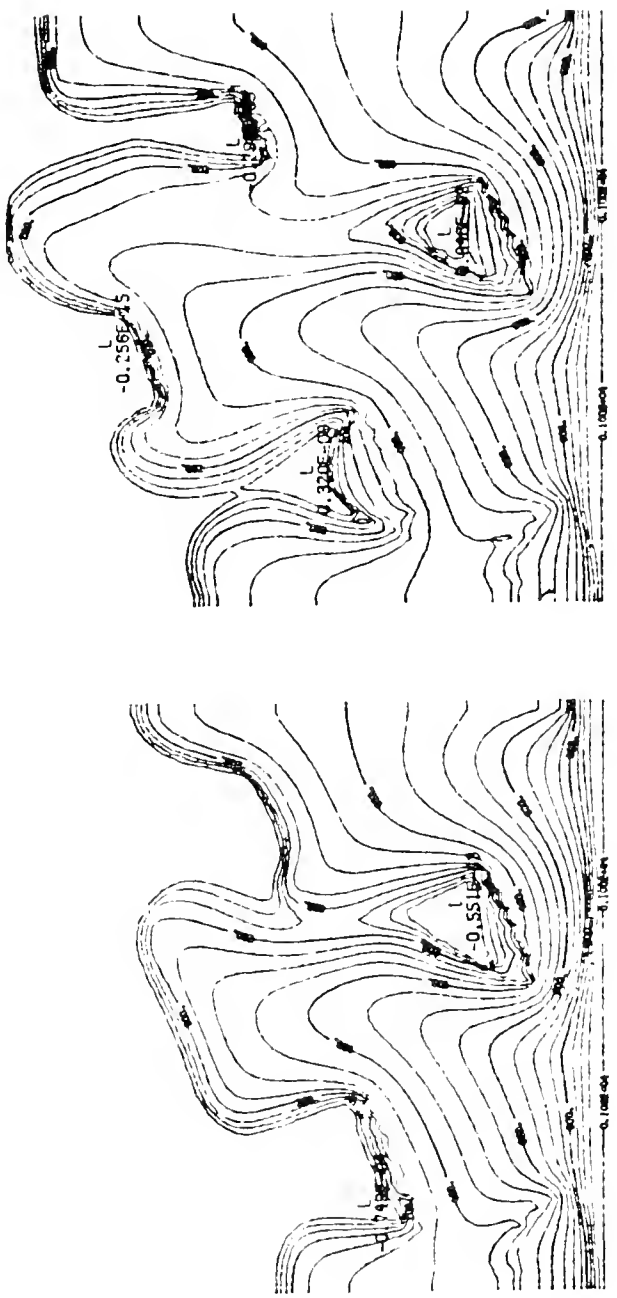

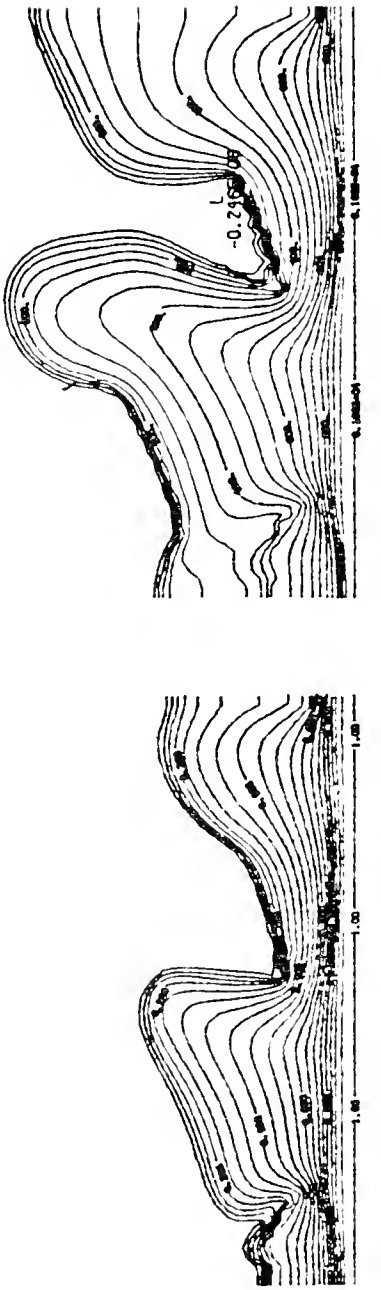

Fig. 8c

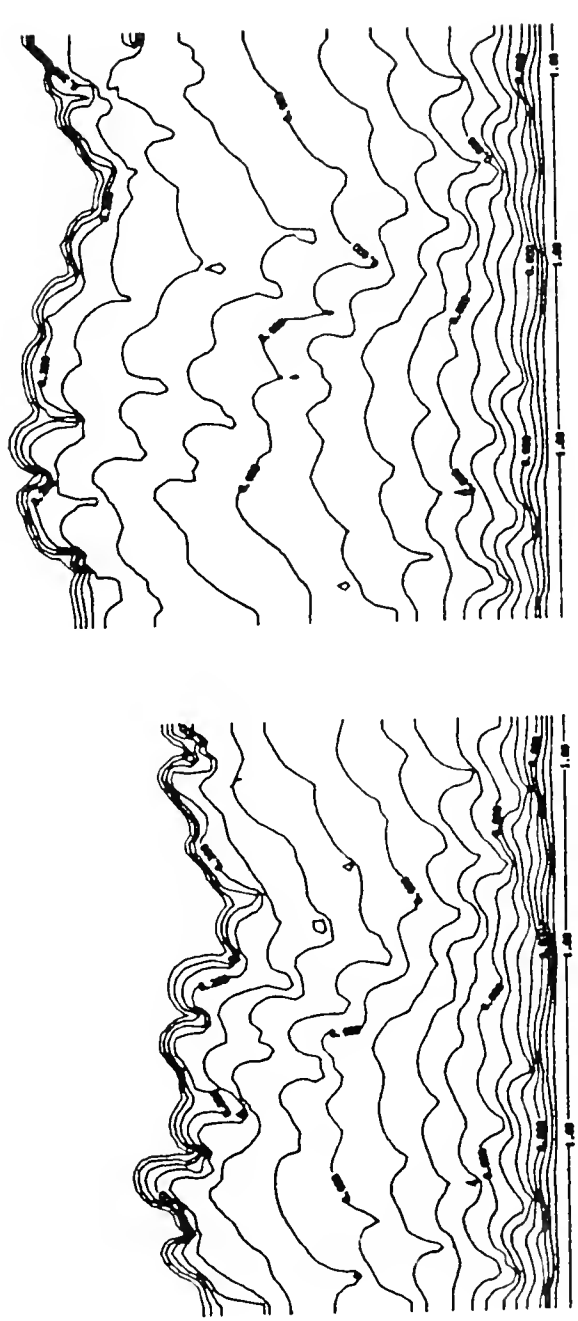

Fig. 8b

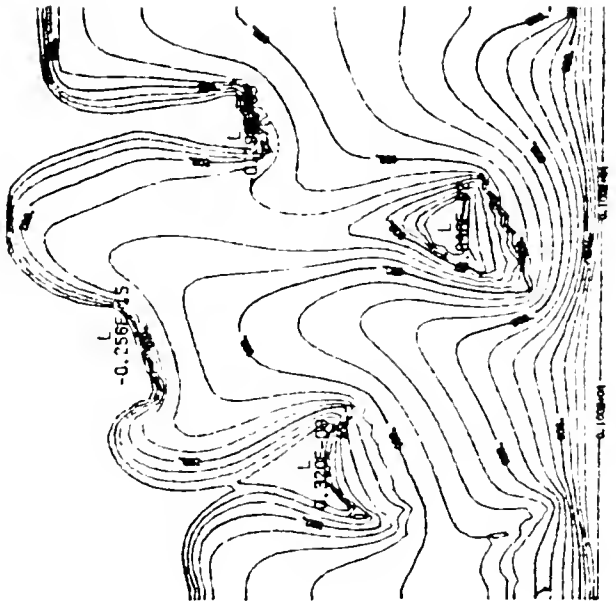

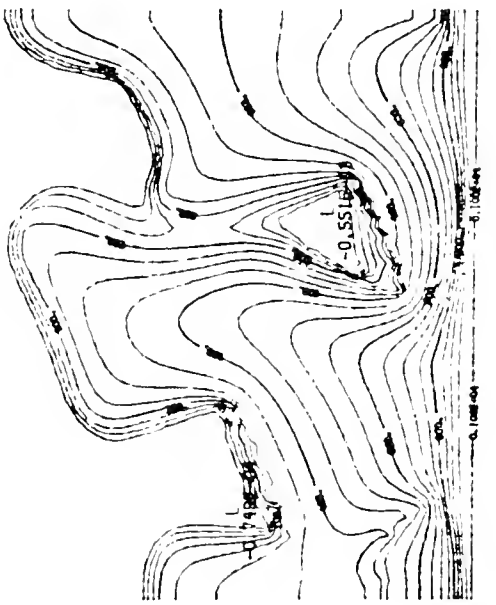

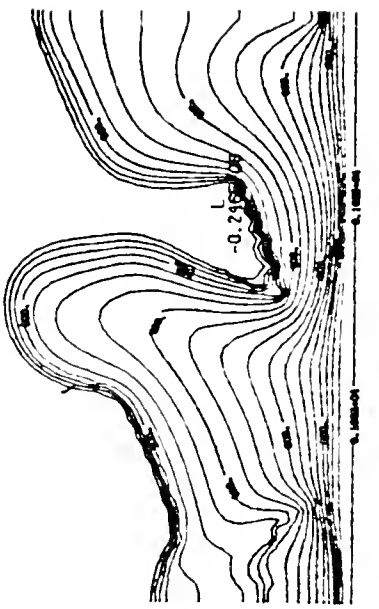

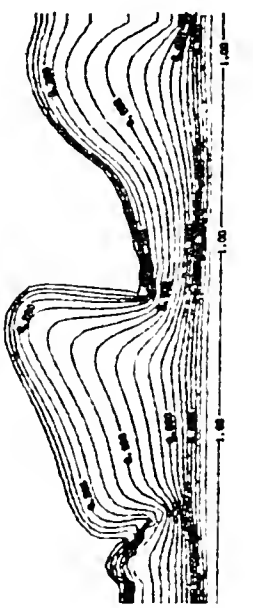

Fig. 8c

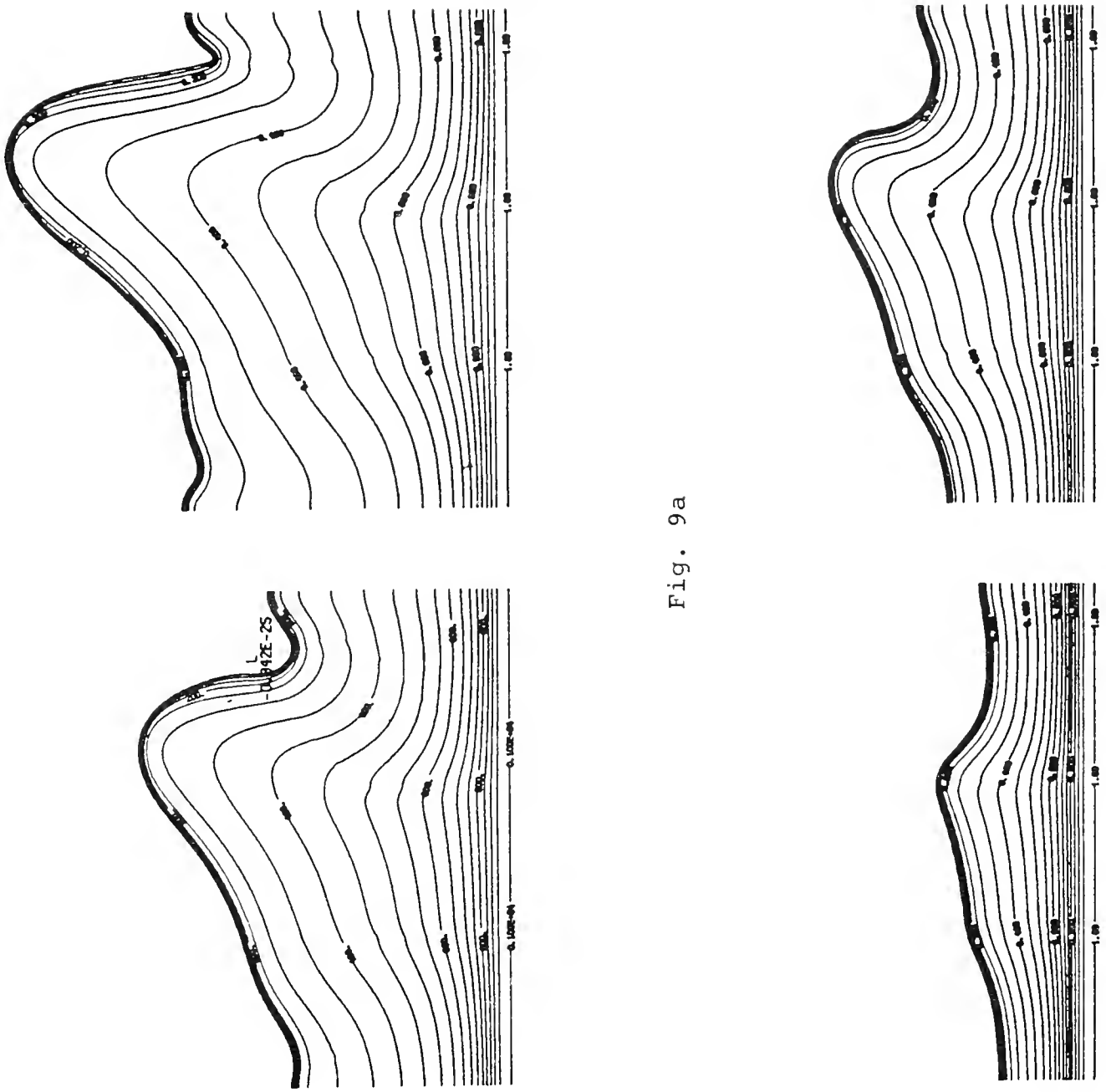

Fig. 9a

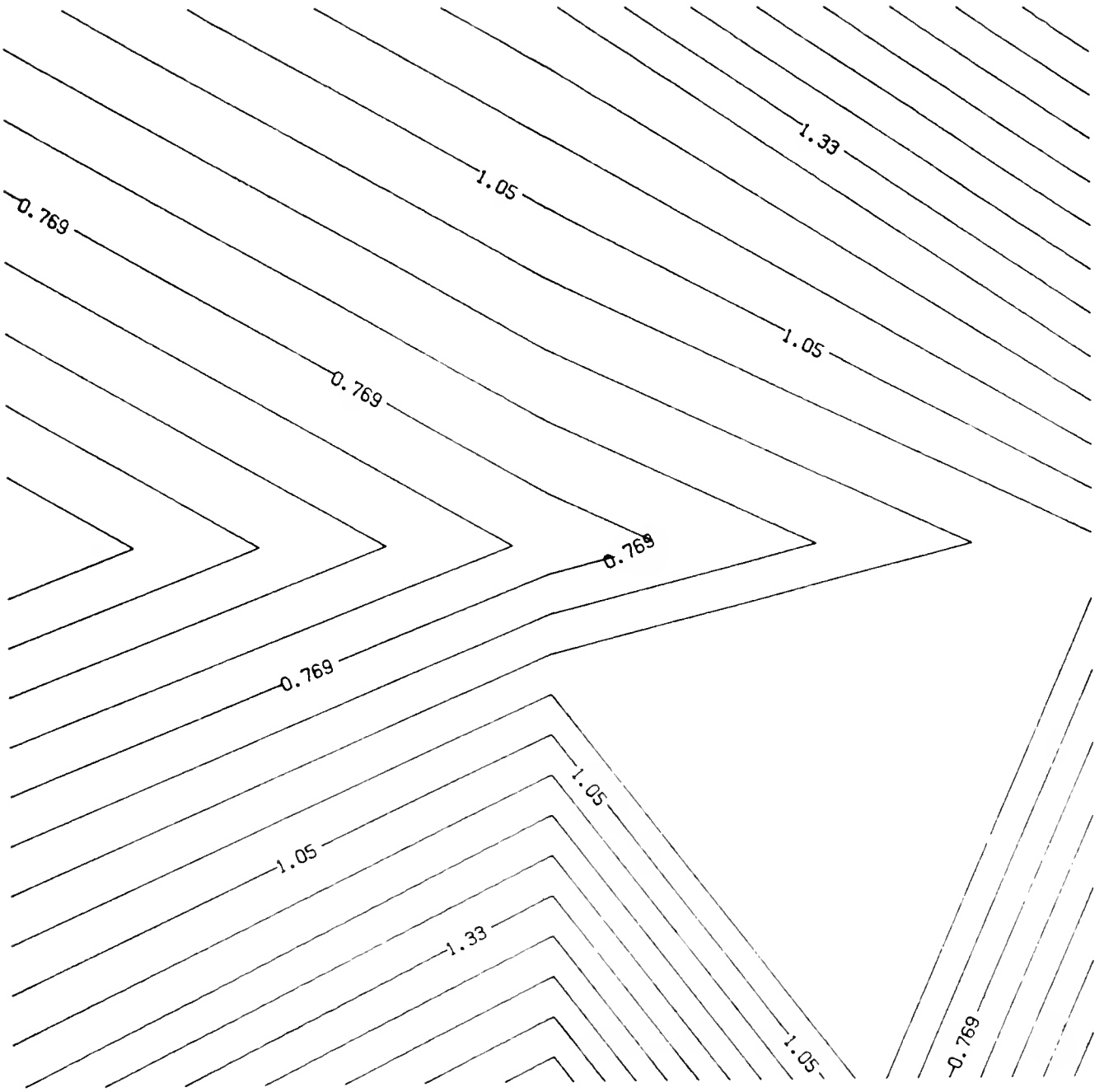

Fig. 9b

This book may be kept

JUN 05 1985

FOURTEEN DAYS

A fine will be charged for each day the book is kept overtime.

GAYLORD 142			PRINTED IN U.S.A.

NYU DOE/ER 03077-244 c.2
King, Michael J
Stability of two
dimensional immiscible...

LIBRARY
N.Y.U. Courant Institute of
Mathematical Sciences
251 Mercer St.
New York, N. Y. 10012